NASA Technical Memorandum 104264

Ground Vibration and Flight Flutter Tests of the Single-Seat F-16XL Aircraft With a Modified Wing

David F. Voracek

June 1993

National Aeronautics and
Space Administration

NASA Technical Memorandum 104264

Ground Vibration and Flight Flutter Tests of the Single-Seat F-16XL Aircraft With a Modified Wing

David F. Voracek
NASA Dryden Flight Research Facility
Edwards, California

1993

National Aeronautics and
Space Administration

Dryden Flight Research Facility
Edwards, California 93523-0273

CONTENTS

ABSTRACT 1

NOMENCLATURE 1

INTRODUCTION 1

DESCRIPTION OF THE TEST AIRCRAFT 2

TEST OBJECTIVES 2

INSTRUMENTATION 2

TEST PROCEDURES AND DATA ANALYSIS 3
- Ground Vibration Tests 3
- Flight Test 4

RESULTS AND DISCUSSION 4
- Ground Vibration Tests 5
- Flutter Analysis 7
- Flight Test 9

CONCLUDING REMARKS 9

REFERENCES 10

FIGURES 12

APPENDIX 46

ABSTRACT

The NASA single-seat F-16XL aircraft was modified by the addition of a glove to the left wing. Vibration tests were conducted on the ground to assess the changes to the aircraft caused by the glove. Flight flutter testing was conducted on the aircraft with the glove installed to ensure that the flight envelope was free of aeroelastic or aeroservoelastic instabilities. The ground vibration tests showed that above 20 Hz, several modes that involved the control surfaces were significantly changed. Flight test data showed that modal damping levels and trends were satisfactory where obtainable. The data presented in this report include estimated modal parameters from the ground vibration and flight flutter test.

NOMENCLATURE

GVT	ground vibration test
FRF	frequency response function
KEAS	knots equivalent airspeed
MAC	modal assurance criteria
MMIF	multivariate mode indicator function
NACA	National Advisory Committee on Aeronautics
NASA	National Aeronautics and Space Administration
Q	dynamic pressure, lb/ft^2

INTRODUCTION

The National Aeronautics and Space Administration (NASA) Dryden Flight Research Facility has conducted many aircraft ground and flight test programs to determine the aeroelastic stability of new and modified research vehicles (refs. 1 and 2). These programs tested new aircraft (ref. 3) and aircraft that have been structurally modified (refs. 4–8).

The left wing of the single-seat F-16XL aircraft was modified to demonstrate new aerodynamic technologies on a highly swept wing planform at supersonic speeds. A titanium test glove was faired to the left wing with graphite and epoxy. Previous experience with similar gloves on aircraft wings showed frequency shifts in the wing torsion modes that had the potential of lowering the flutter speed (refs. 4 and 5). The structural dynamic concerns for the F-16XL modification were the effects on the aeroelastic and aeroservoelastic characteristics caused by the changes in weight, stiffness, and airfoil shape.

The work discussed in this report assessed the effects of the wing glove on the aeroelastic and aeroservoelastic stability and cleared a flight envelope for the aerodynamic experiments. Previous structural dynamic data documented during the design of the F-16XL did not contain any ground or flight tests of the modified aircraft configuration. So ground vibration and flight tests were required before and after the modification. One ground vibration test (GVT) was performed before the modification for baseline data;

another GVT was performed after the modification for comparison; then flight flutter was tested. The desired envelope for the aerodynamic experiments was a dynamic pressure of 533 lb/ft^2 up to an altitude of 32,000 ft, then increasing Mach number at 32,000 ft to a dynamic pressure of 1008 lb/ft^2 up to the temperature limit (160 °F) of the glove design. The flutter clearance was the final proof of the aeroelastic and aeroservoelastic stability of the aircraft.

This report describes the approach taken to flight-qualify the aircraft modification, which includes the aircraft configuration, test instrumentation, data analysis techniques, and test procedures used to perform the baseline and modified aircraft GVTs and flight flutter clearance. The measured differences in modal frequencies and mode shapes of the aircraft were sufficient to warrant a flight flutter clearance. The report includes the results of the flight tests, which consist of modal frequency and damping estimated during flight with the glove mounted on the left wing.

DESCRIPTION OF THE TEST AIRCRAFT

The F-16XL aircraft tested is the single-seat version (fig. 1) powered by a Pratt & Whitney (West Palm Beach, Florida) F100-PW-200 engine. The inboard wing leading edge is swept 70° and the outboard wing leading-edge is swept 50°. The aircraft is capable of speeds near Mach 2 and altitudes up to 60,000 ft. Inert missiles are carried on the inboard wing station for center-of-gravity ballast, and the wingtips are configured with launcher rails only (ref. 9).

The basic aircraft was modified by installing a titanium test glove that was faired to the left wing with graphite and epoxy (fig. 1). The total added weight of the modification was 207 lb. The glove design incorporated a modified NACA airfoil. The test glove extended from the forward spar on the lower wing surface around the leading edge to the 25–40 percent chord line on the upper wing surface. The glove fairing extended to the trailing edge spar on the upper surface (ref. 10).

TEST OBJECTIVES

There were two main objectives for the ground vibration and flight flutter tests of the F-16XL. The first objective was to assess the effect of the wing glove and its associated hardware on the structural characteristics of the F-16XL. The second objective was to establish a flight envelope free of any flutter or aeroservoelastic instability.

INSTRUMENTATION

Different instrumentation was used to perform these tests, depending on the purpose of the test. For vibration testing on the ground, piezoelectric accelerometers were attached to the aircraft to measure the response of the structure. Each of the 180 accelerometers had a nominal sensitivity of 1000 mV/*g* and weighed 3 gm. The mounting block for each accelerometer weighed approximately 10 gm and was attached to the aircraft by hot glue. The accelerometer locations are listed at the end of this paper in an appendix (table A-1 and figs. A-1 through A-4). An HP9000/380 workstation and HP3565 data-acquisition and analysis system (figs. 2(a) and 2(b)) acquired, filtered, displayed, and recorded 183 channels of data (3 force inputs and 180 accelerometer responses).

Three electrodynamic shakers capable of generating a maximum force of 150 lb were used to excite the aircraft. One shaker was placed aft on the right wing launcher rail (fig. 3); a second shaker was placed forward on the left wing launcher rail; and a third shaker was suspended from an overhead crane and attached to the vertical stabilizer (fig. 4). The vertical stabilizer shaker suspension cables were long enough to ensure that the pendulum frequency of the shaker was well below the resonant frequencies of the aircraft. The shakers were attached to the aircraft with a telescoping thrust rod, a stinger, and a force link. The force link was attached to a locking ball nut joint that was mounted to the aircraft (fig. 5).

For flight testing, the aircraft was instrumented with seven accelerometers. Figure 6 shows the locations of these accelerometers. All accelerometers were sampled at 200 samples/sec and had a range of $\pm 10\ g$, except the vertical tail which had a range of $\pm 25\ g$.

The accelerometer responses were telemetered from the aircraft to the NASA Dryden Spectral Analysis Facility for near-real-time stability monitoring. Selected accelerometers were routed to a spectrum analyzer for real-time frequency domain information during the test points. A Fourier analyzer provided near-real-time frequency and damping information for critical accelerometer responses (ref. 2). Other relevant flight information such as Mach number, altitude, and airspeed were displayed on video monitors.

TEST PROCEDURES AND DATA ANALYSIS

The procedures for conducting each test and methods of analyzing data also differed depending on the purpose of the test. The following sections describe these procedures and methods.

Ground Vibration Tests

The GVTs were conducted on an essentially flight-ready aircraft. Some equipment that was not yet installed was simulated by ballast weights placed as close to the proper locations as possible. All structural panels were fastened and the canopy closed and locked. The aircraft was on its landing gear during the test and the struts were collapsed to eliminate potential nonlinearities. The tires were deflated to one-half the normal pressure to provide a softer support. Fuel loading for both tests consisted of full fuselage tanks and empty wing tanks. The control surfaces were in the trim position for each test and potential nonlinearities caused by excessive actuator freeplay in the elevons and ailerons was minimized by suspending approximately 50 lb of lead shot from the surfaces with an elastic bungee cord. The bungee cord was used to decouple the dynamics of the lead shot from the aircraft.

Two GVTs were performed on the aircraft—one before the glove installation (baseline GVT) and a second after (modified GVT). The general procedure for each GVT was to install accelerometers on the aircraft and then connect them to a digital data-acquisition system with some signal conditioning. The aircraft was excited by three electrodynamic shakers using uncorrelated random signals with a frequency content of 1 to 50 Hz. Frequency response functions (FRFs) were estimated and subsequently used to determine the structural frequencies and mode shapes below 30 Hz.

The data were analyzed by estimating the aircraft's modal parameters of frequency, damping, and mode shape, and then by comparing the baseline and modified GVT results for significant modal changes. The identification of the modal frequencies was simplified by using all 540 FRFs (3 inputs and 180 responses) in the calculation of the multivariate mode indicator functions (MMIFs) for each configuration.

The MMIF is essentially a multi-input–multi-output formulation of the classical method of tuning normal modes. A normal mode response phase lags the sinusoidal excitation by 90° (ref. 11) at resonance, and the MMIF identifies this resonance frequency. It also identifies repeated roots. The MMIF consists of one function for each reference or excitation input to the structure. Three inputs were used to excite the F-16XL during the GVTs. The primary MMIF has minimum values at the modal frequencies. If the secondary function has significant minima corresponding to the same frequencies of the primary MMIF, this suggests the presence of repeated roots. The number of minima at a particular frequency corresponds to the multiplicity of the roots (refs. 11 and 12). The MMIF reduces the analysis time to identify the structural modes by using all 540 FRFs simultaneously rather than each individually.

The MMIFs were correlated with the individual FRFs to identify and tabulate all the modes of the aircraft. The modal parameters were estimated by a single-degree-of-freedom technique that fits a second-order polynomial to the FRFs in a selected frequency range. Then the modal parameters and mode shapes from the baseline and the modified GVTs were compared using the modal assurance criteria (MAC), which is an orthogonality check of the structural modes (ref. 12). A MAC value close to unity suggests that the modes have the same shape, and a value near zero implies that the mode shapes are independent. The GVT results also were compared with a previously existing baseline database from the aircraft manufacturer and were assessed for any unusual vibratory motion of the airplane or potential aeroelastic concerns.

Flight Test

The flight-flutter clearance was accomplished by obtaining test data at 14 test points (fig. 7) flown in order of increasing dynamic pressure over a series of three flights. At each test point, data were obtained during 60 sec of stabilized flight. Atmospheric turbulence provided structural excitation. Because of the lack of turbulence at some test points, a series of pilot-induced control surface pulses supplemented the turbulence excitation. The accelerometer responses were monitored in real time for any aircraft instabilities and were used for near-real-time modal frequency and damping calculations. These results were then evaluated before clearing the aircraft to the next test point.

Near-real-time and postflight data analysis consisted of calculating the autopower spectra. Then a frequency range of interest was identified and the rest of the spectrum was set to zero. The inversed Fourier-transformed was performed on the spectrum and an exponential window was applied. Transformation back to the frequency domain resulted in a smoothed spectrum from which a half-power method was used to estimate the structural frequency and damping (ref. 13).

Because the time available for data analysis was restricted during flight, the data were more thoroughly analyzed between flights using the same reduction techniques. Postflight analysis established confidence levels in estimated modal frequency and damping values by providing more estimates and using statistical averages and variances on the results. It also provided the opportunity for further manipulation of the data, such as addition and subtraction of wingtip sensor data to enhance symmetric and antisymmetric motion, which also aided in separating closely spaced modes.

RESULTS AND DISCUSSION

The GVT results showed close comparison of the structural frequencies and mode shapes between the baseline and modified aircraft. Some fuselage modes could not be identified because of the lack of fuselage excitation. Three significant modal frequency and mode shape changes in the control surface modes

caused some concern because of a possible control surface buzz problem. Results indicated additional flutter analyses were not necessary. The flight test results show adequate damping trends for the modes that could be identified. Some structural frequency and damping estimates could not be extracted from the response spectra because of the lack of random atmospheric turbulence for excitation at these frequencies. The pilot-induced raps and kicks did not increase excitation to improve the frequency and damping estimates. The detailed results from the ground vibration and flight-flutter tests will be covered in the following sections.

Ground Vibration Tests

The MMIFs (figs. 8 and 9) from the baseline and modified aircraft identified 14 to 15 modes between 5 and 30 Hz. Only the primary and secondary MMIFs are shown from each GVT. The baseline MMIF (fig. 8) shows 11 distinct modes up to 25 Hz. Four modes between 25 and 30 Hz are not as distinct but are present. The secondary MMIF in the baseline MMIF shows a distinct frequency drop corresponding to the same frequency of 7.9 Hz as the primary MMIF, which suggests the presence of a repeated root. The modified aircraft MMIF shows nine modes between 5 and 25 Hz. Again the four modes between 25 and 30 Hz are present but not as distinguishable as the other nine modes. No repeated roots were estimated. Table 1 summarizes the structural frequencies from the MMIF.

Table 1. Multimode indicator function (MMIF) structural frequencies.

Baseline aircraft GVT		Modified aircraft GVT
Primary	Secondary	
7.9	7.9	8.0
9.8		9.7
10.7		10.8
12.4		12.5
13.2		13.2
13.6		13.6
16.2		20.5
18.6		21.7
20.2		23.9
21.7		25.3
22.2		26.5
26.4		27.6
27.6		28.5
28.8		

The structural frequencies identified from the MMIF were correlated with the FRFs from the baseline and modified aircraft GVTs. Figures 10–12 show the driving point FRFs from both GVTs. These three FRFs show little change in frequency between the two GVTs. There are slight frequency shifts below 15 Hz, which is to be expected because of the added mass of the glove. These frequency shifts become greater above 15 Hz, as is shown in the right-wing FRF (fig. 11).

The individual FRFs do not show all the structural frequencies that can be seen in the MMIF. The baseline MMIFs show three modes at 9.6, 16.2, and 18.6 Hz that are not present in the FRFs. The double root calculated in the baseline MMIF and several structural frequencies above 20 Hz also are not seen in the FRFs. Using the MMIF, therefore, can greatly simplify the identification of structural frequencies.

Modal parameter estimation identified 12 structural frequencies and mode shapes. A comparison of frequencies estimated from the baseline and modified aircraft is shown in Table 2. The third column in the table shows the MAC value between the baseline and modified GVT mode shape results. Figures 13–24 show the mode shapes for the baseline and modified GVTs.

Table 2. Baseline and modified GVT frequency comparison and MAC values.

Mode name	Baseline GVT frequency, Hz	Modified GVT frequency, Hz	MAC mode comparison
Symmetric wing bending	7.975	8.037	0.990
Symmetric launcher rail bending	13.695	13.885	0.996
Symmetric control surface mode 1	21.738	21.525	0.838
Symmetric control surface mode 2	26.423		
Antisymmetric wing bending	10.793	10.895	0.991
Vertical tail bending	12.480	12.555	0.993
Antisymmetric launcher rail bending	13.242	13.233	0.948
Antisymmetric control surface mode 1	20.359	20.569	0.807
Antisymmetric control surface mode 2	22.194	23.986	0.488
Antisymmetric control surface mode 3	27.049	27.811	0.817
Antisymmetric control surface mode 4	28.776	28.650	0.295
Asymmetric control surface mode 1	27.169	26.616	0.808

The three mode shapes at 9.6, 16.2, and 18.6 Hz and the double root estimated from the MMIF are not shown in Table 2. These modes where identified as fuselage bending modes from the manufacturer's GVT data and flight tests (refs. 14–16). Adequate mode shapes could not be estimated for these structural frequencies because of the lack of excitation on the fuselage during the baseline and modified aircraft GVTs.

The frequency and mode shapes that could be identified show very little change between the baseline and modified GVTs. The fundamental aircraft modes, such as first symmetric and antisymmetric wing bending, show about a 1-percent change in frequency and the MAC values are 0.99 and above. Although

most of the GVT data show close agreement between the baseline and modified GVT, three significant differences in the control surface modes may be noted.

The first difference is the absence of a 26.4-Hz symmetric control surface mode in the modified aircraft GVT data. Figure 16 shows the baseline mode shape. The absence of this mode in the modified aircraft data is likely a result of the changes in the wing mass and stiffness caused by the addition of the glove. Figure 16 shows that the control surface mode has considerable deflection at the wing leading edge and inboard wing area. The glove covers this area of the wing and its mass and stiffness substantially reduce the modal response to the control surface deflections.

The second difference was identified in the second antisymmetric control surface mode. The data in Table 2 indicate an 8-percent shift in frequency from 22.2 to 24.0 Hz and a poor mode shape comparison. Figure 21 shows the mode shape. As was seen in the symmetric 26.4 Hz control surface mode, this mode has significant inboard wing motion on both the right and left wings. Again, the addition of the glove is in an area where the baseline GVT showed significant deflections. The total effect in the modified aircraft is stiffening, thereby reducing the deflection and increasing the frequency. The differences in the mode shapes are reflected in the MAC comparison. The change in mode shape was restricted to the glove area, so the vertical stabilizer and the fuselage motion remained unchanged.

The third and final difference in the modal data was observed in the fourth antisymmetric control surface mode (fig. 23). The mode shape comparison shows a low MAC value of 0.295. The mode shape is asymmetric now but originally was antisymmetric. One possible explanation is that the 26.4-Hz symmetric mode (fig. 16) was shifted up to 28 Hz because of the glove and coupled with the 28.8-Hz antisymmetric mode. The distinct changes in mode shape before and after the modification resulted in the low MAC value.

A review of the GVT data showed no change in frequency in the range where the structural notch filters were active in the flight control system. Therefore, there were no aeroservoelastic concerns for this modification to the aircraft.

Flutter Analysis

The flutter analysis data from the manufacturer of the unmodified F-16XL aircraft (table 3) shows the antisymmetric flutter frequencies for the different fuel and wingtip store configurations range from 23.5 to 29.2 Hz (ref. 16). For the specific launcher-rails-only configuration, the flutter frequencies range from 23.5 to 25.3 Hz. Figure 25 shows the manufacturer's analysis and flight test points. The flutter speeds for these configurations were predicted to be outside the structural design limits of the aircraft, so no new flutter analysis was completed on the modified F-16XL.

The addition of the glove affected the control surface modes above 20 Hz, which were predicted to have the lowest flutter speeds by the flutter analysis performed during the design of the F-16XL. Changes in the control surface modes raised concerns about a control surface buzz which occurs in the transonic flight region for most aircraft. These changes and concerns coupled with the fact that the launcher-rails-only configuration was never flight-tested for flutter were important in planning the test requirements of the modified aircraft.

Table 3. Flutter analysis for baseline aircraft (from Ref. 10).

			Subsonic (Mach 0.9)		Subsonic (Mach 0.9)		Supersonic (Mach 1.2)		Supersonic (Mach 1.2)	
			Symmetric		Antisymmetric		Symmetric		Antisymmetric	
Fuselage fuel	Wing fuel	Wingtip store	Minimum velocity, KEAS	Frequency, Hz	Minimum velocity, KEAS	Frequency, Hz	Minimum velocity, KEAS	Frequency, Hz	Minimum velocity, KEAS	Frequency, Hz
Full	Empty	Clean	1022	13	939	24.6	1260	28.8	880	25.9
Full	Half full	Clean	1084	12.2	863	24	1164	28	835	26.1
Full	Empty	Launcher	1047	13.3	924	23.9	1377	18.1	874	24.5
Full	Half full	Launcher	1162	11.5	763	23.5	1299	18.9	805	25.3
Full	Empty	Aim-9L	1165	11.8	792	23.9	1333	12.5	965	26
Full	Half full	Aim-9L	1146	11.3	774	24.8	1329	12.3	953	29.2

Flight Test

During the original flight flutter clearance of the F-16XL only two wingtip configurations were flown: clean tip and launcher rail with missiles. These configurations were cleared to a maximum dynamic pressure of 1700 lb/ft^2. The clean tip was also flown to a maximum of 1.6 Mach at 30,000 ft. Figure 25 shows the maximum speeds flown during the first flutter clearance of the F-16XL at several altitudes. All test points were flown outside the NASA-desired flight envelope. The glove program consists of a launcher-rails-only configuration, which was not flight-tested.

Flutter data were acquired at 25,000 and 38,000 ft with Mach numbers ranging from 0.70 to 1.8. Figures 26–38 show the accelerometer response spectrums for Mach 0.90 at both test altitudes. Figures 39–49 are plots of the frequency and damping estimates as functions of Mach number. Trends for frequency and damping were only clear for six structural modes. The missing frequency and damping data could not be extracted from the response spectra because of the lack of random atmospheric turbulence for excitation at these frequencies even with the pilot-induced raps and kicks. The accelerometer spectra show some energy was imparted in the 20-Hz range (figs. 27–31). However, individual modes above 15 Hz were impossible to distinguish because of the noise and a lack of clean excitation in the modal frequency range. This was a concern, since the original aircraft flutter analysis showed that the antisymmetric modes above 20 Hz exhibited the lowest flutter speeds and the GVT results showed significant change with these structural frequencies. Although the energy imparted above 15 Hz was small and damping values and trends could not be established, it was felt that monitoring accelerometer responses on the strip charts would allow flutter testing to proceed safely.

The modal frequency and damping estimates were satisfactory. In figure 41 an adverse trend is evident at Mach 1.1 and above. The real-time monitoring of these modes did not indicate that a structural instability was near. The damping values are considered conservative using atmospheric turbulence as the only excitation. In reference 17, an experiment comparing forced structural excitation with random atmospheric turbulence showed that random atmospheric turbulence produced damping values that were lower by about a factor of 2.

The envelope cleared for the experiment was an airspeed of 400 knots up to an altitude of 32,000 ft, then a maximum speed of 605 knots through 38,000 ft, and finally a maximum speed of 1.75 Mach above 38,000 ft. This slightly smaller envelope from the project envelope was given because it is easier for a pilot to maintain airspeed than dynamic pressure. Figure 45 shows this envelope.

CONCLUDING REMARKS

The F-16XL aircraft was modified by mounting a titanium glove on the left wing. As a result of the modification, the possibility of an aeroelastic or aeroservoelastic instability existed. To alleviate the concern, several tests were performed to study the effects of the glove on the aircraft's structural dynamics.

A ground vibration test was performed on the aircraft before and after the glove installation on the left wing to determine the effects of the stiffness and mass change on the modal characteristics. The results showed that the modal frequencies and mode shapes below 20 Hz did not significantly change. Above 20 Hz, several modes that involved the wing control surface motion were significantly changed.

The flight flutter test showed that the aircraft was free from any aeroelastic and aeroservoelastic instabilities within the flight envelope. Insufficient in-flight structural excitation prevented the identification and tracking of fuselage modes and several critical structural modes above 15 Hz. The stability of the structural modes for which frequency and damping could not be determined was maintained through real-time monitoring of the accelerometer responses. In spite of this lack of excitation, a safe and efficient flight flutter clearance program was accomplished.

Dryden Flight Research Facility
National Aeronautics and Space Administration
Edwards, California, April 12, 1993

REFERENCES

1. Kehoe, Michael W., *Aircraft Ground Vibration Testing at NASA Ames-Dryden Flight Research Facility*, NASA TM-88272, July 1987.

2. Kehoe, Michael W., *Aircraft Flutter Testing at the NASA Ames-Dryden Flight Research Facility*, NASA TM-100417, May 1988.

3. Kehoe, Michael W., *Flutter and Aeroservoelastic Clearance of the X-29A Forward-Swept Wing Airplane*, NASA TM-100447, Sept. 1989.

4. Kehoe, Michael W., *Flutter Clearance of the F-14 Variable-Sweep Transition Flight Experiment Airplane - Phase 1*, NASA TM-88287, Sept. 1987.

5. Freudinger, Lawrence C. and Michael W. Kehoe, *Flutter Clearance of the F-14A Variable-Sweep Transition Flight Experiment Airplane - Phase 2*, NASA TM-101717, July 1990.

6. Cazier, F.W. Jr. and M.W. Kehoe, *Ground Vibration Test of an F-16 Airplane With Modified Decoupler Pylons*, NASA TM-87634, Apr. 1986.

7. Freudinger, Lawrence C., *Flutter Clearance of the F-18 High-Angle-of-Attack Research Vehicle With Experimental Wingtip Instrumentation Pods*, NASA TM-4148, Oct. 1989.

8. Kehoe, Michael W. and Joseph F. Ellison, *Flutter Clearance of the Schweizer 1-36 Deep-Stall Sailplane*, NASA TM-85917, Aug. 1985.

9. Bensinger, C.T., "F-16XL Flight Flutter Tests," General Dynamics 400PR100, July 20, 1983.

10. Anderson, Bianca T. and Marta Bohn-Meyer, *Overview of Supersonic Laminar Flow Control Research on the F-16XL Ships 1 and 2*, NASA TM-104257, Oct. 1992.

11. Williams, R., J. Crowley, and H. Vold, "The Multivariate Mode Indicator Function in Modal Analysis," Third International Modal Analysis Conference, Jan. 1985.

12. I-DEAS Test User's Guide, Structural Dynamics Research Corporation, 1990.

13. Craig, Roy R., "Structural Dynamics: An Introduction To Computer Methods," John Wiley & Sons Inc., New York, 1981.

14. Adams, R.S. and J.C. Elrod, "F-16XL Ground Vibration Test No. 2 (Air-To-Ground)," General Dynamics 400PR083, December 20, 1982.

15. Adams, R.S. and J.C. Elrod, "F-16XL Ground Vibration Test No. 1 (Air-To-Air)," General Dynamics 400PR066, July 9, 1982.

16. Ellis, J.A., "Flutter Analysis of F-16XL Air-To-Air Configurations," General Dynamics 400PR062, June 28, 1982.

17. Vernon, Lura, *In-flight Investigation of a Rotating Cylinder-Based Structural Excitation System for Flutter Testing*, NASA TM-4512, June 1993.

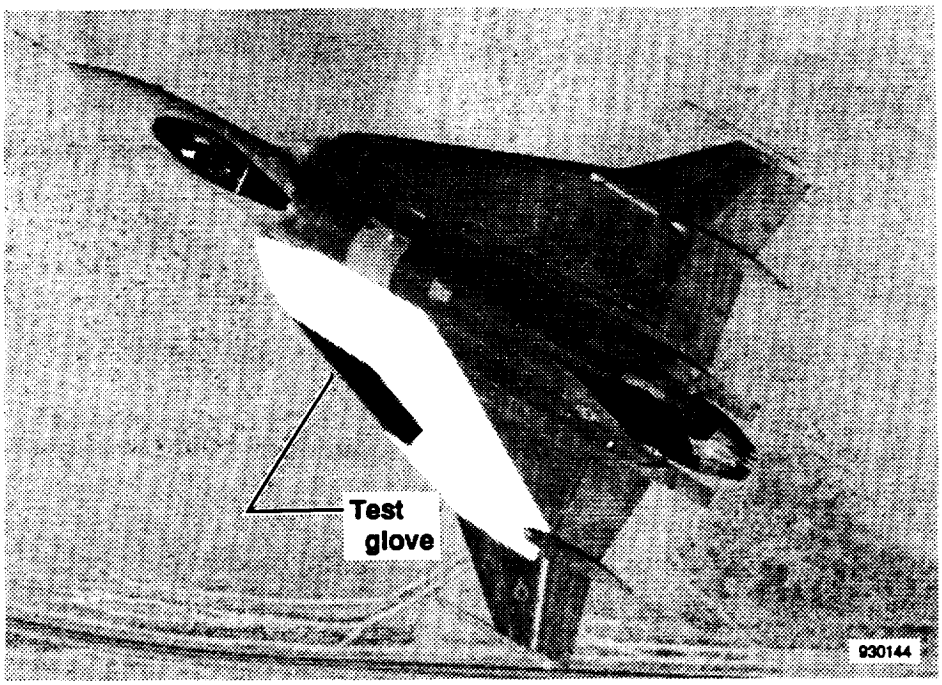

Figure 1. NASA F-16XL single-seat aircraft with the test glove installed on the left wing.

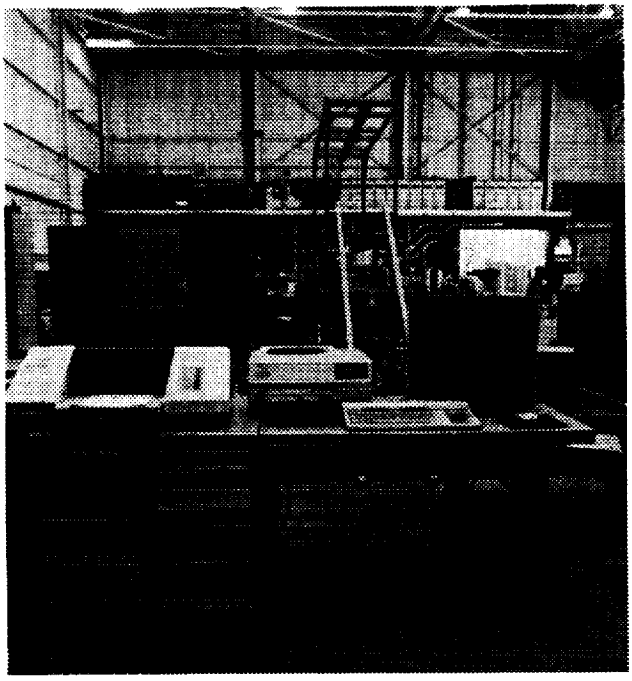

EC91-391-5

(a) The HP9000/380 workstation.

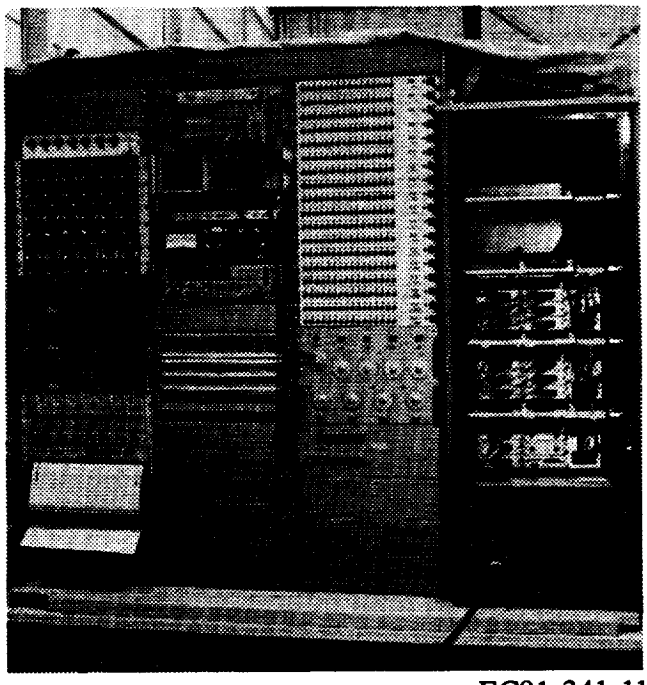

EC91-341-11

(b) The HP3565 data-acquisition and analysis system.

Figure 2. Structural analysis test system.

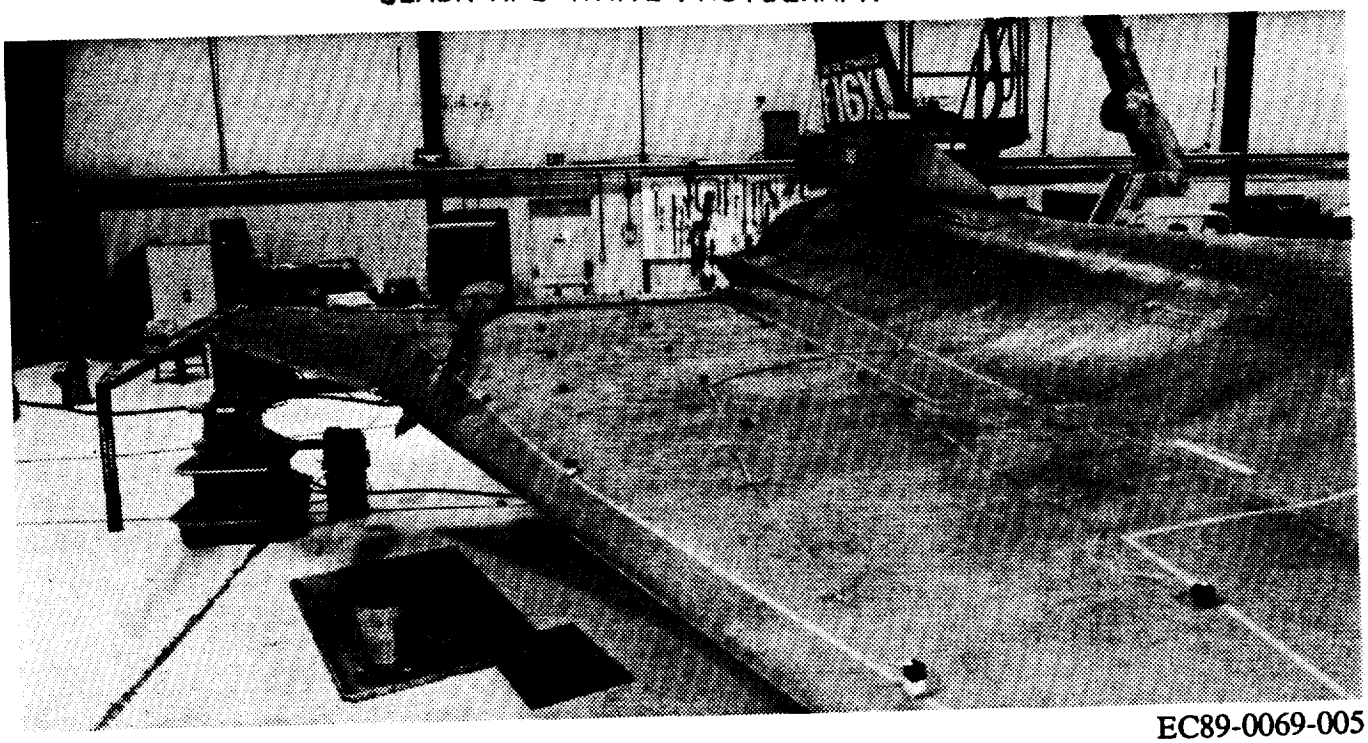

EC89-0069-005

Figure 3. GVT right-wing setup.

EC89-0069-003

Figure 4. GVT vertical-tail setup.

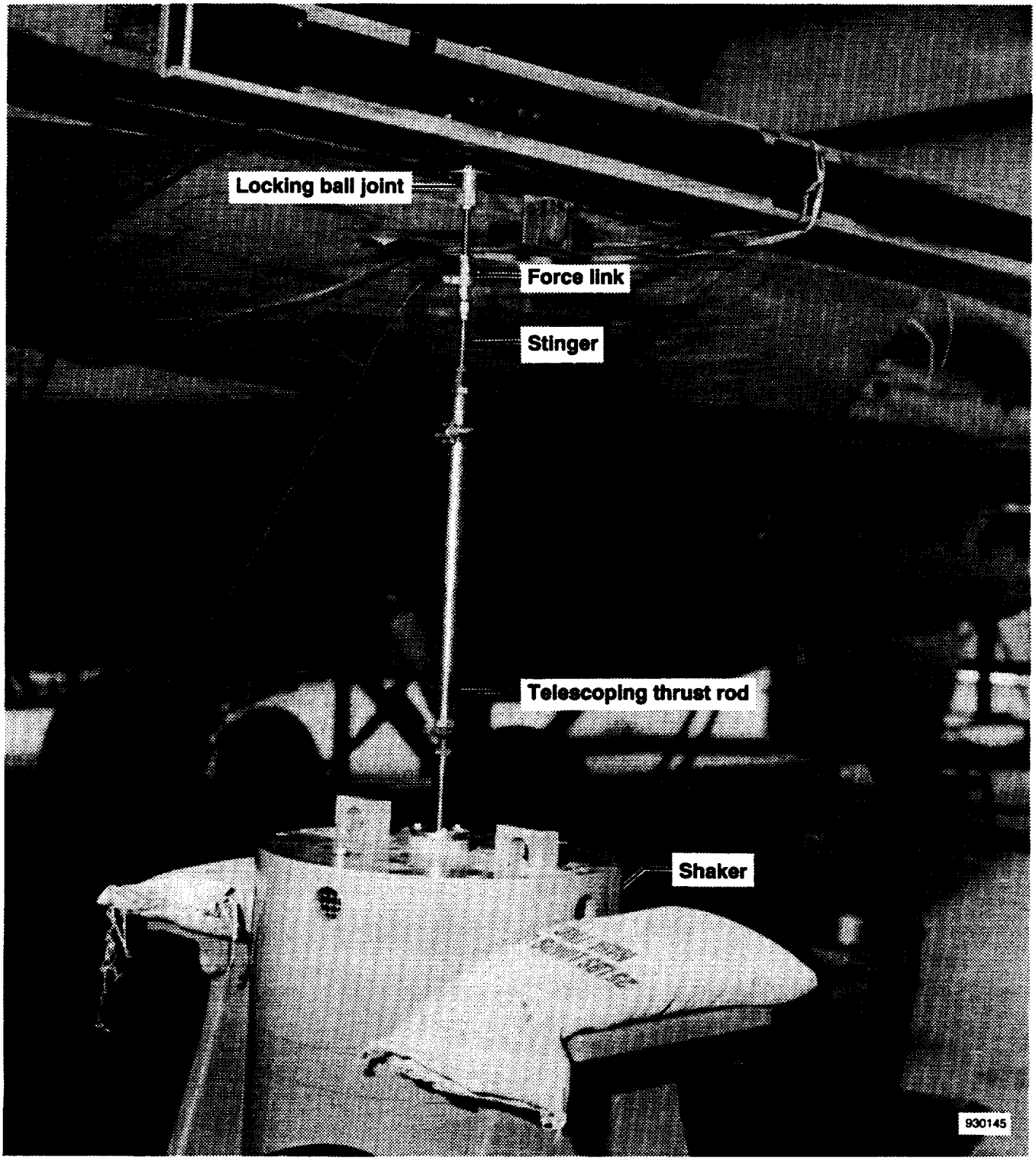

Figure 5. GVT excitation shaker setup.

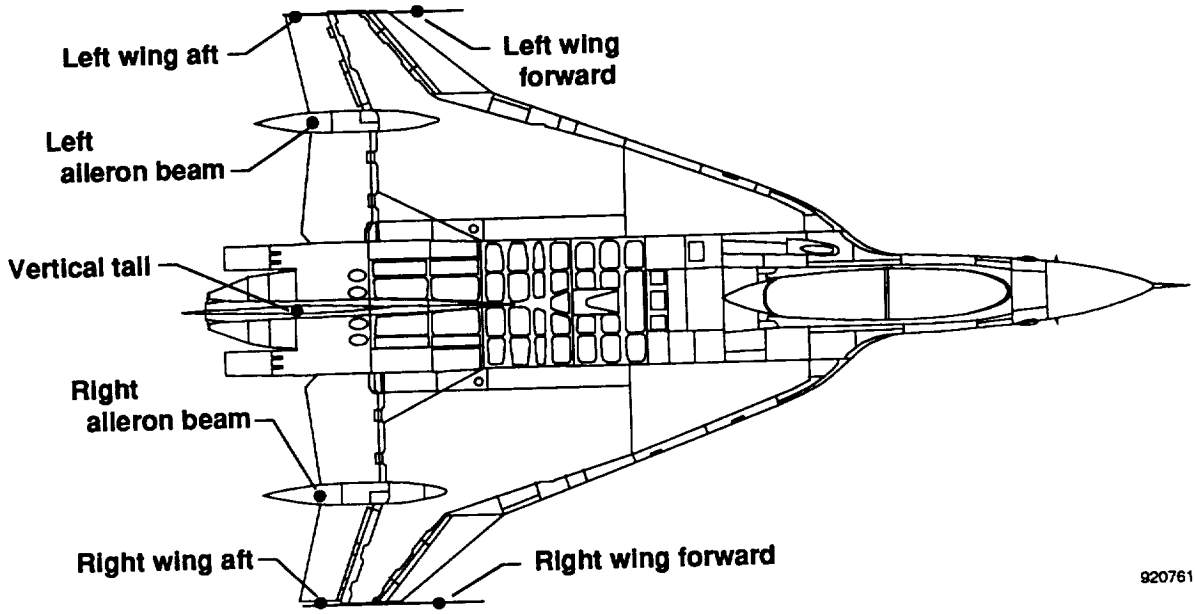

Figure 6. Flight test acceleromoter locations.

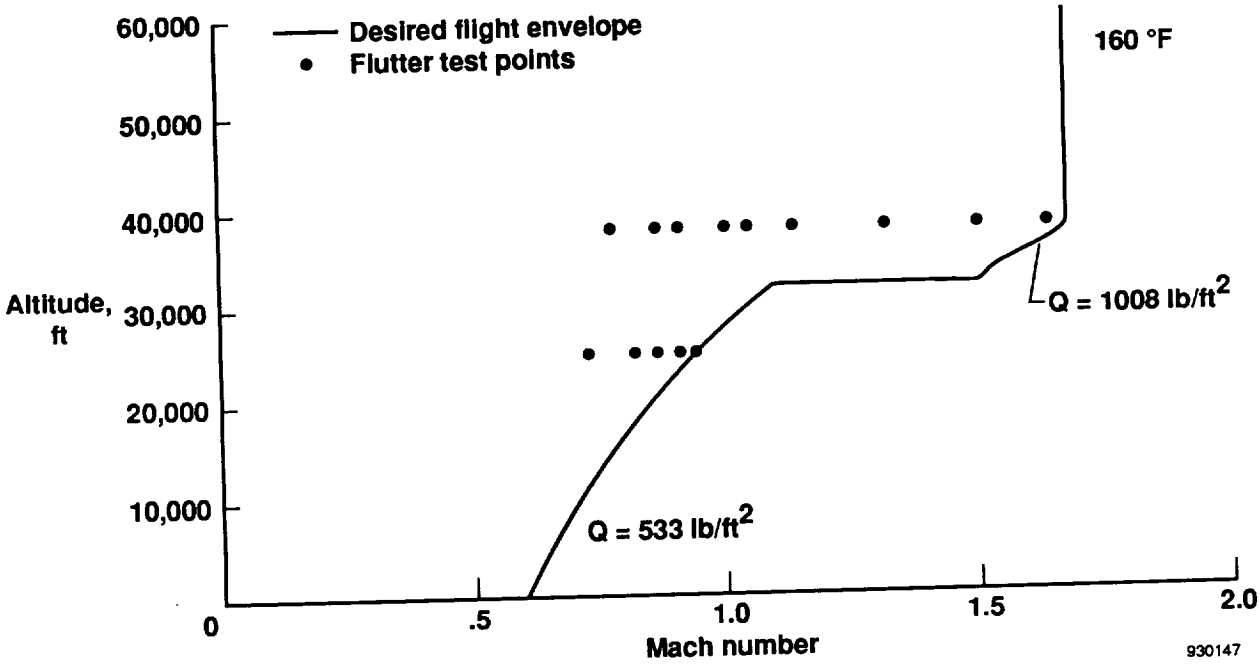

Figure 7. Flight flutter test points and desired flight envelope.

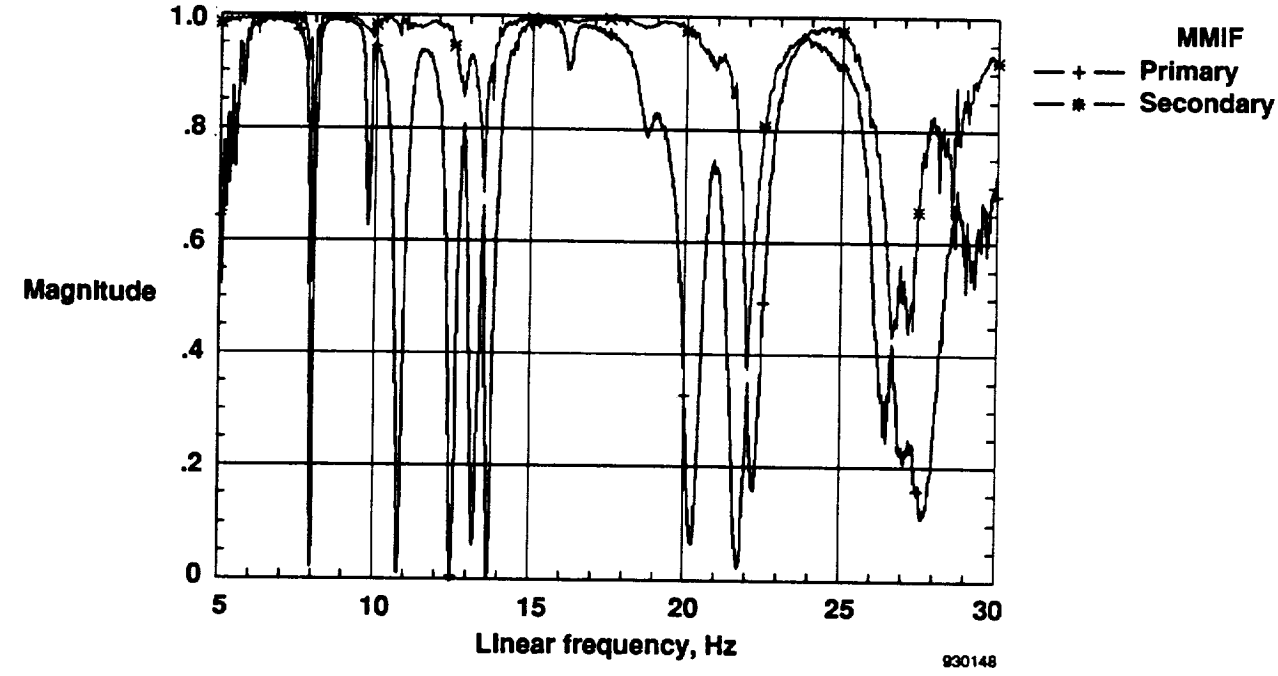

Figure 8. Baseline aircraft MMIF.

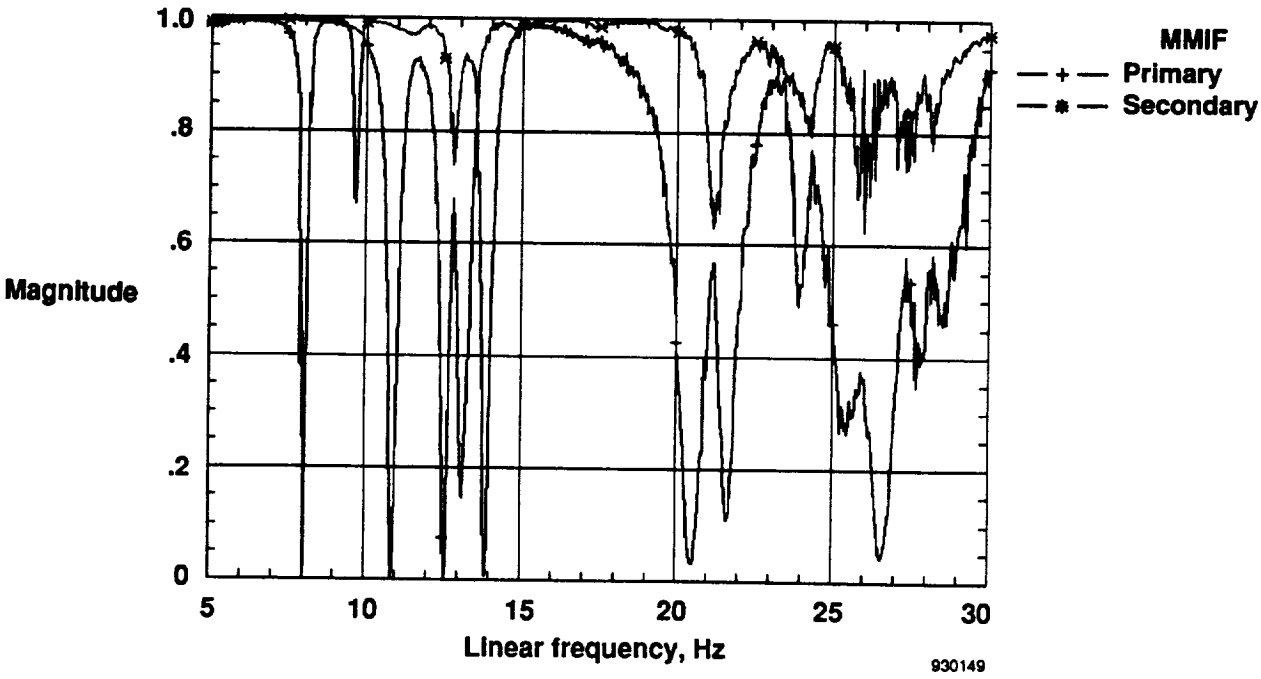

Figure 9. Modified aircraft MMIF.

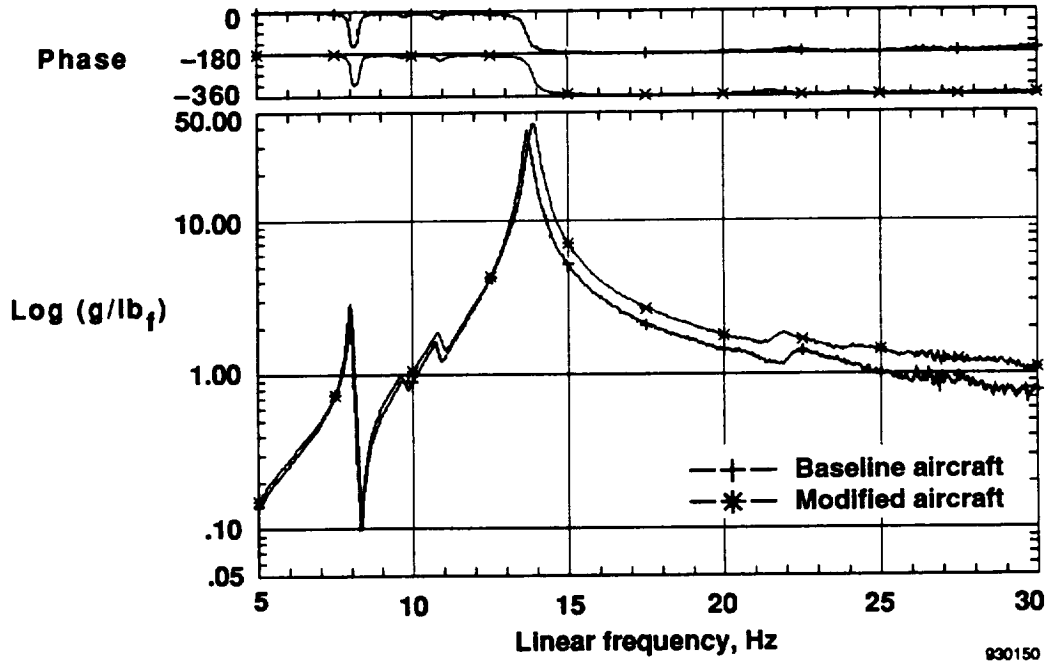

Figure 10. Left-wing driving point accelerometer FRF.

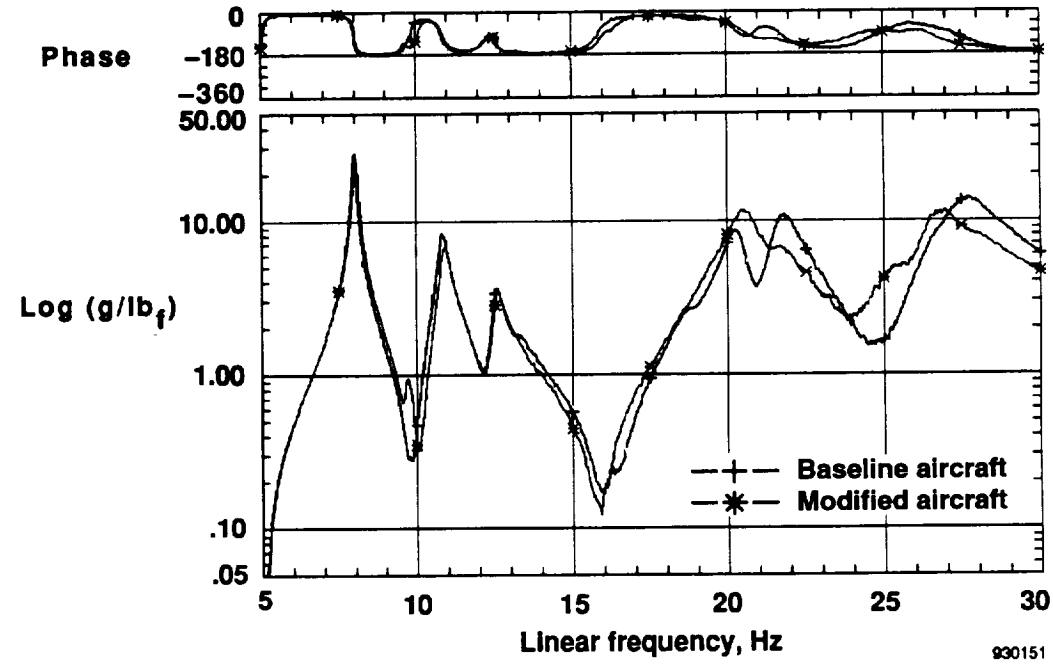

Figure 11. Right-wing driving point accelerometer FRF.

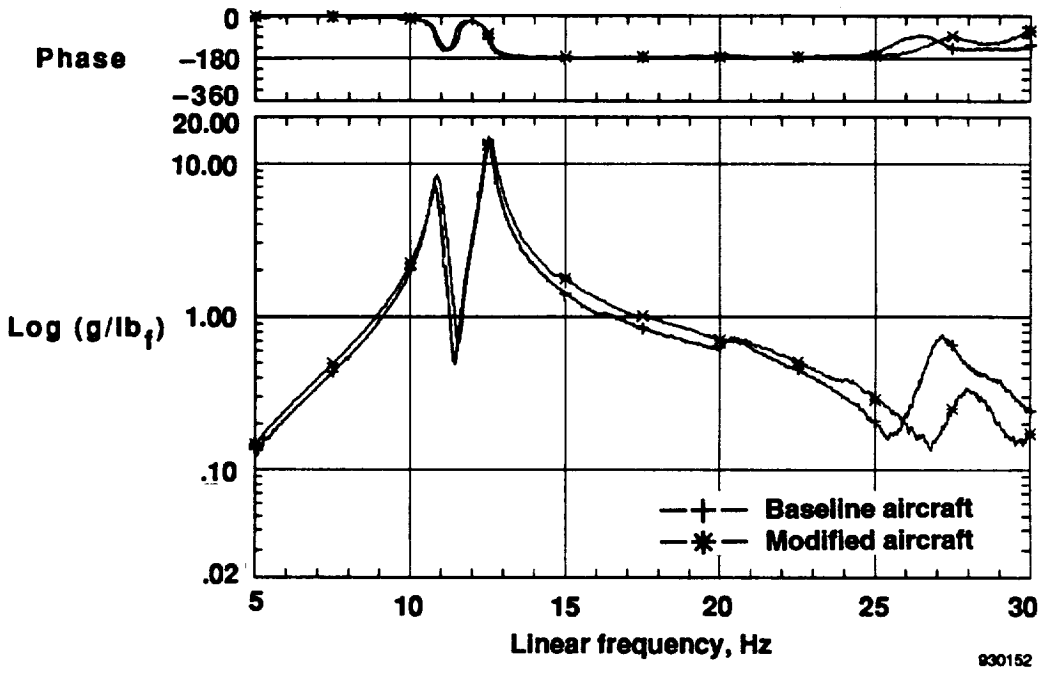

Figure 12. Vertical-tail driving point accelerometer FRF.

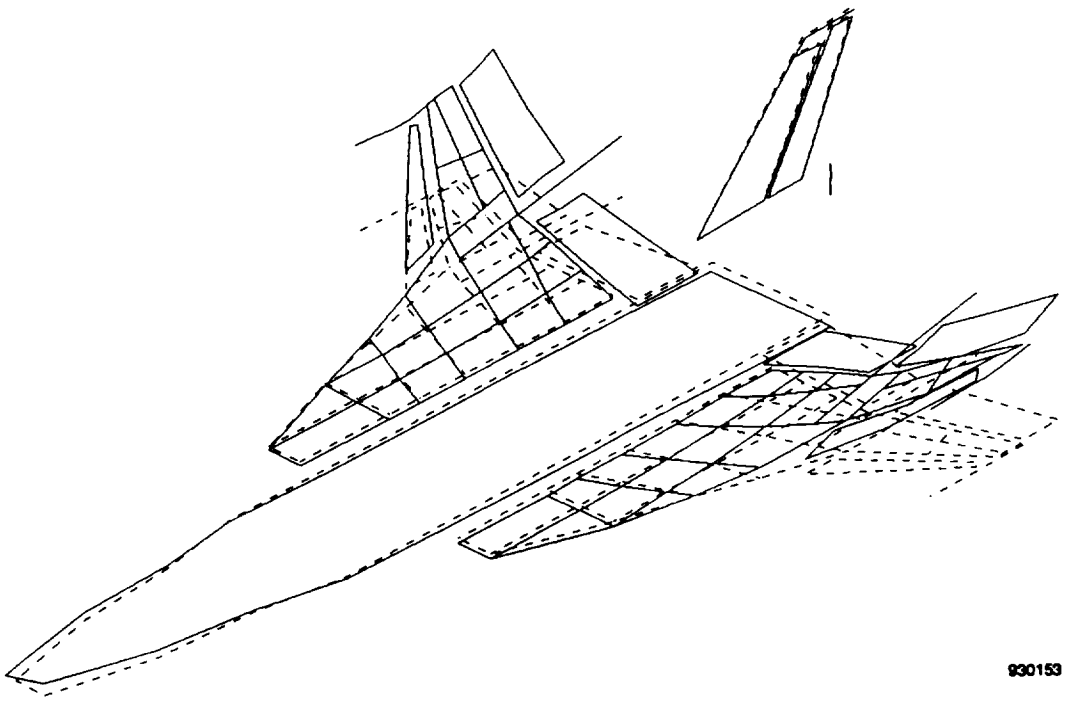

(a) Baseline, 7.98 Hz.

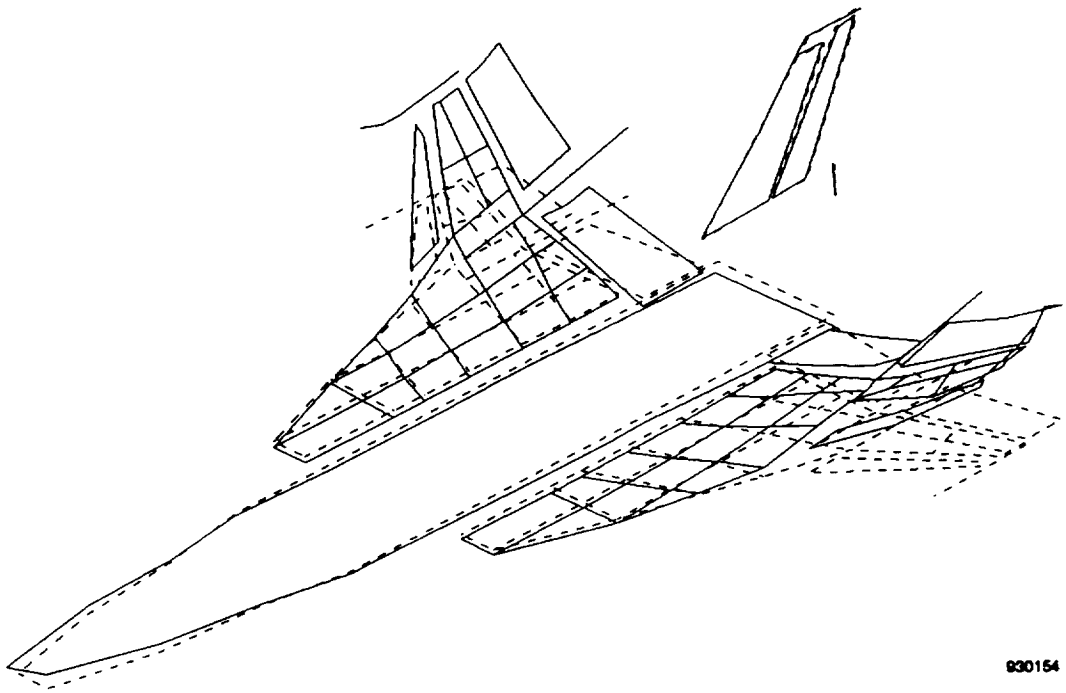

(b) Modified, 8.04 Hz.

Figure 13. Aircraft mode shapes, symmetric wing bending.

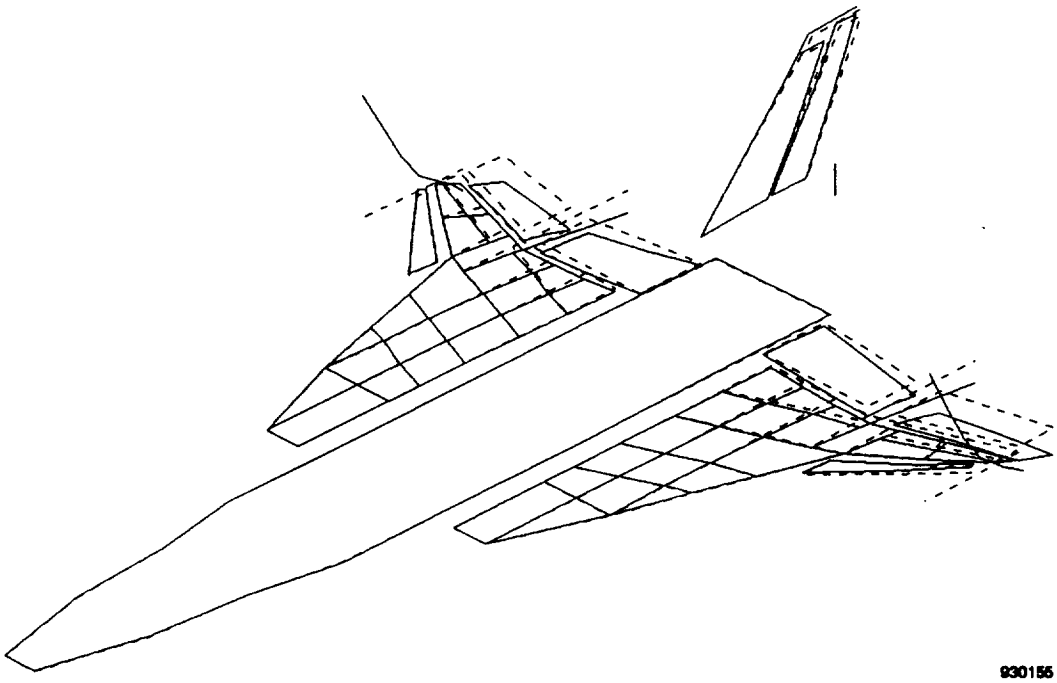

(a) Baseline, 13.69 Hz.

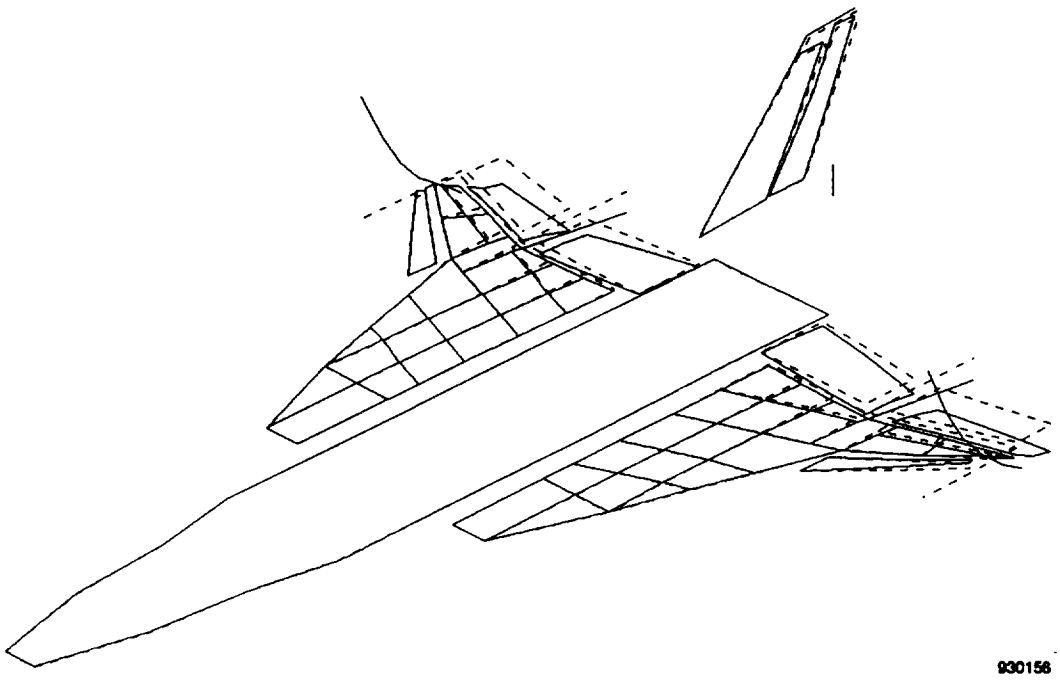

(b) Modified, 13.88 Hz.

Figure 14. Aircraft mode shapes, symmetric launcher rail bending.

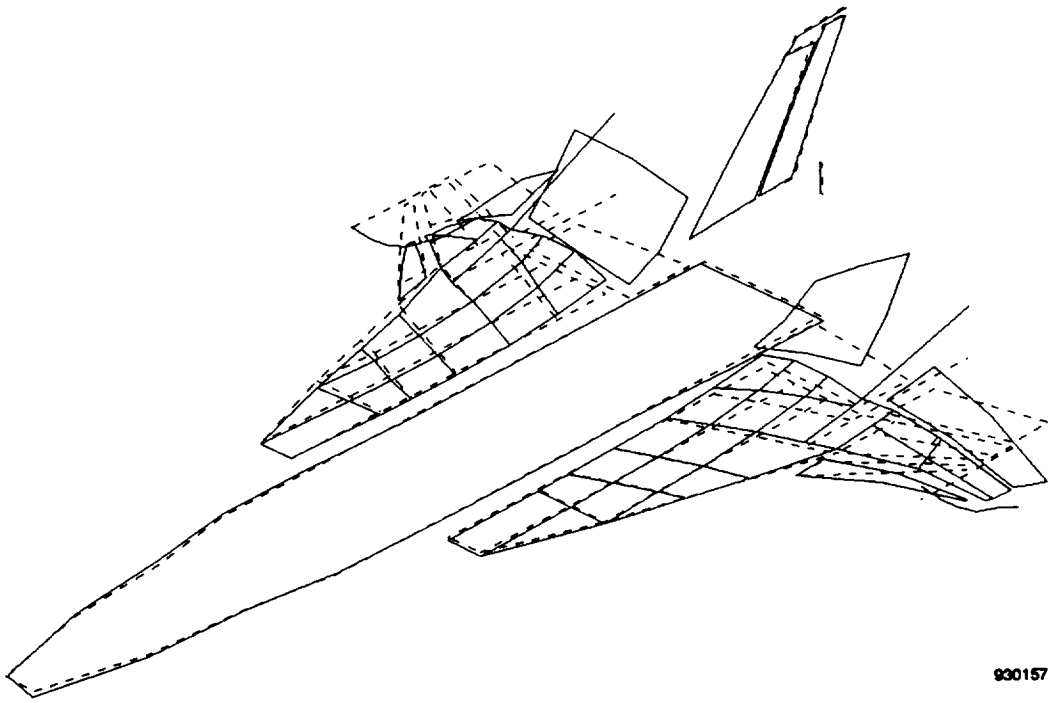

(a) Baseline, 21.74 Hz.

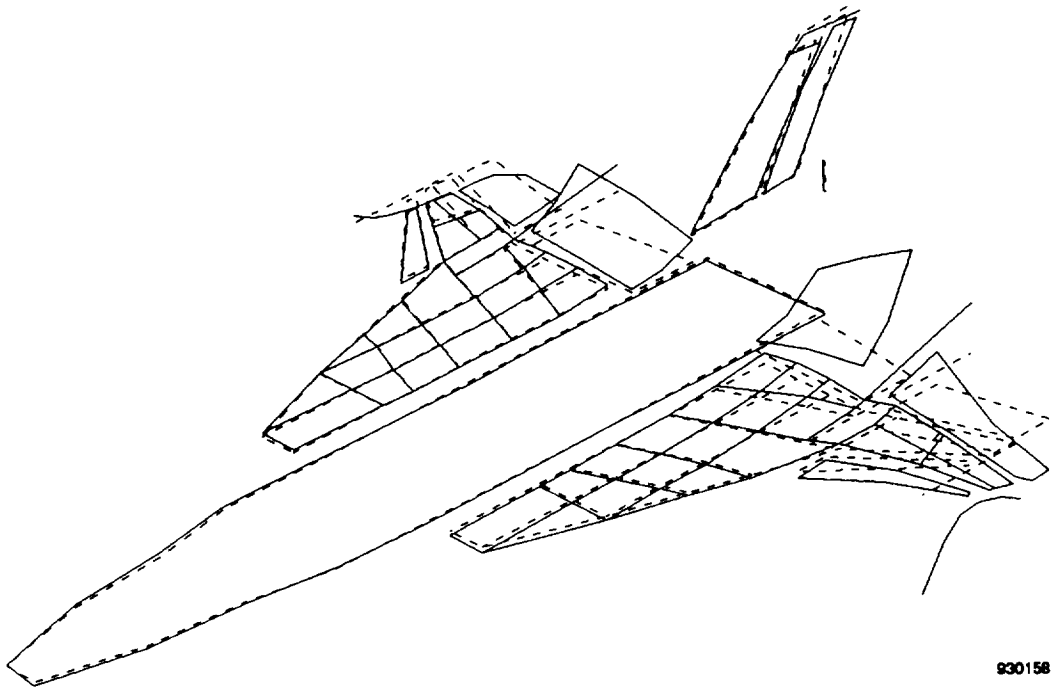

(b) Modified, 21.53 Hz.

Figure 15. Aircraft mode shapes, symmetric control surface mode 1.

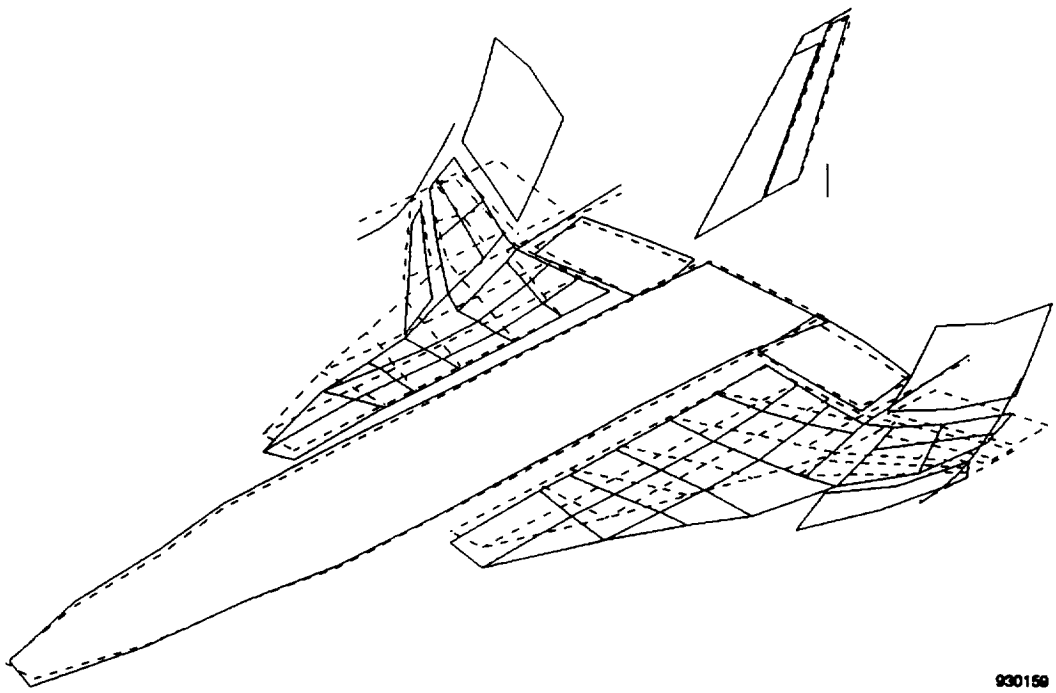

(a) Baseline, 26.42 Hz.

Mode shape could not be estimated.

(b) Modified.

Figure 16. Aircraft mode shapes, symmetric control surface mode 2.

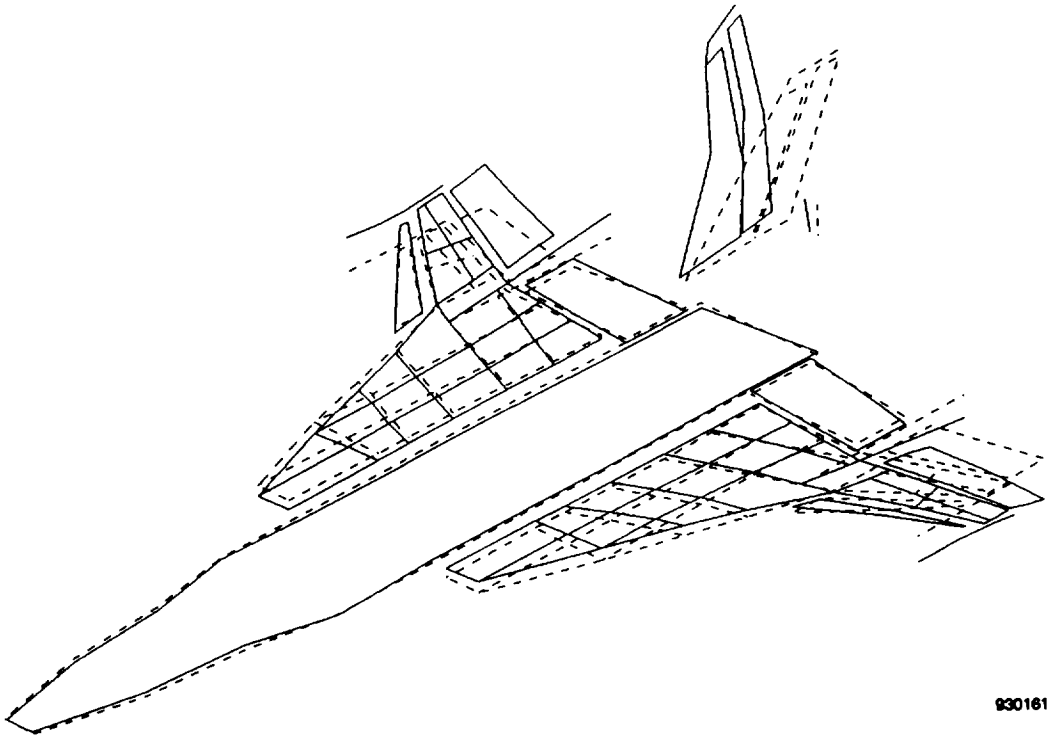

(a) Baseline, 10.79 Hz.

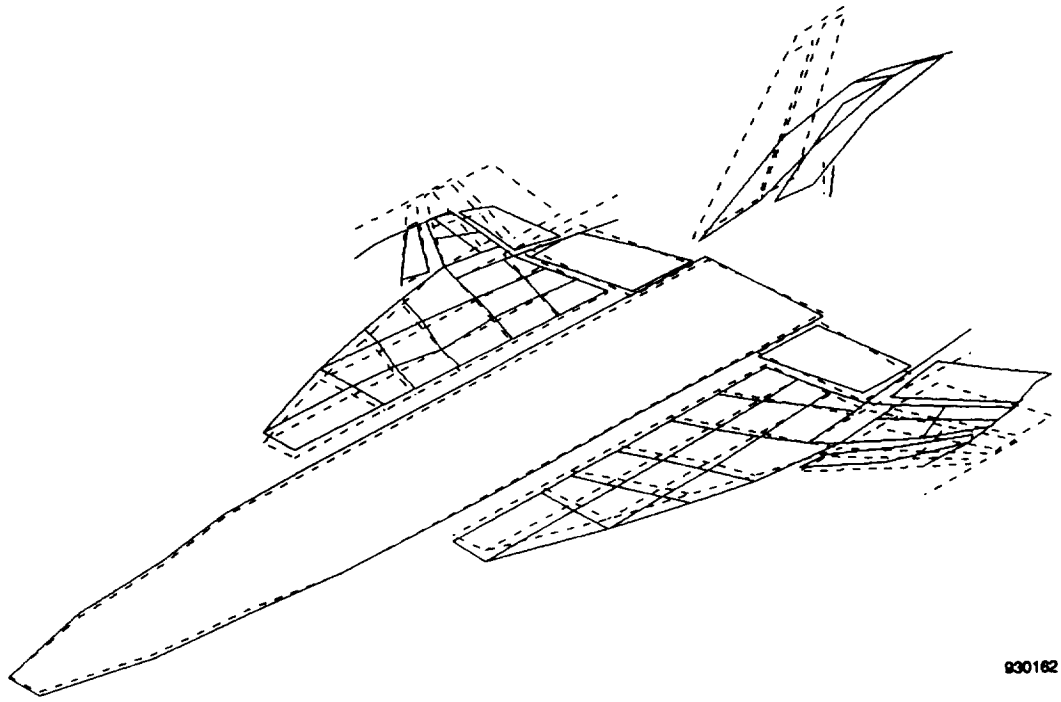

(b) Modified, 10.90 Hz.

Figure 17. Aircraft mode shapes, antisymmetric wing bending.

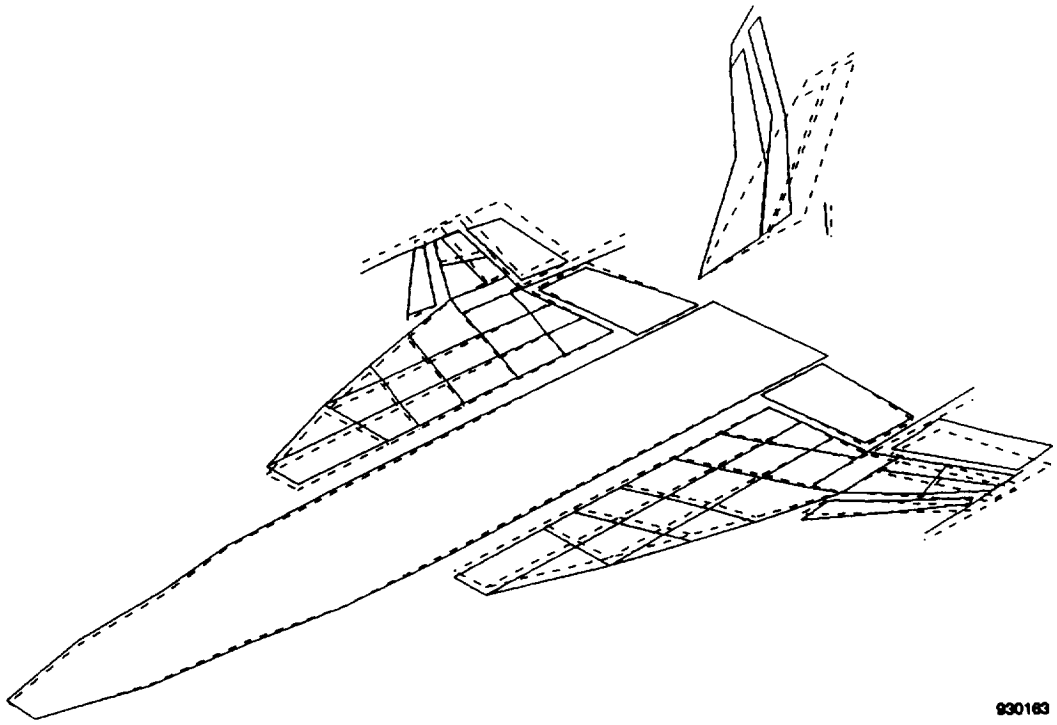

(a) Baseline, 12.48 Hz.

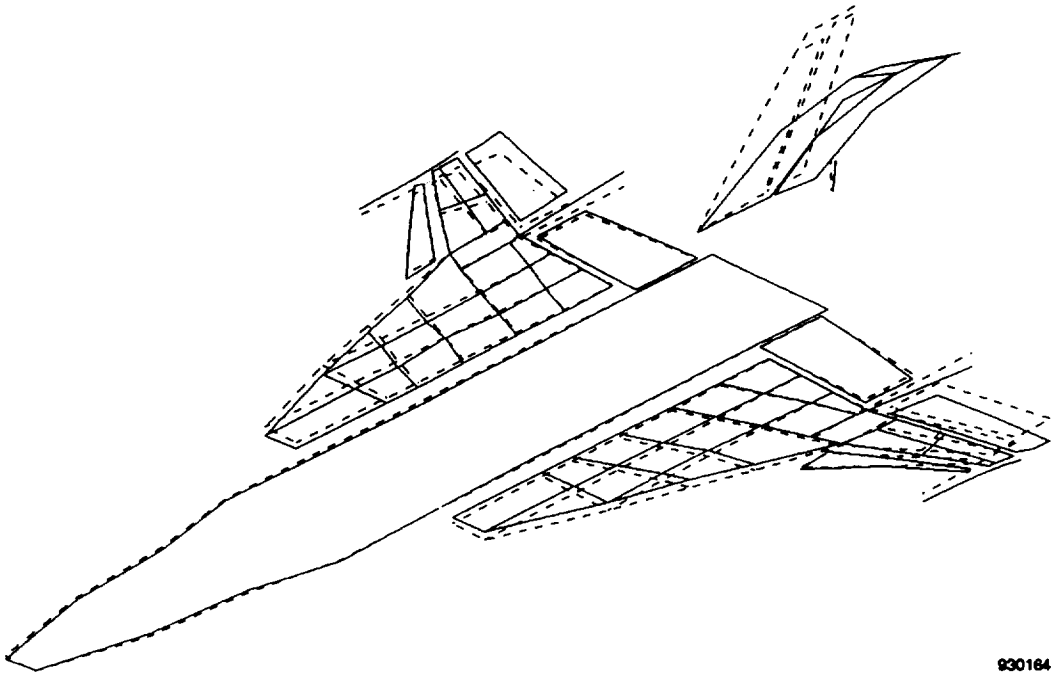

(b) Modified, 12.56 Hz.

Figure 18. Aircraft mode shapes, vertical tail bending.

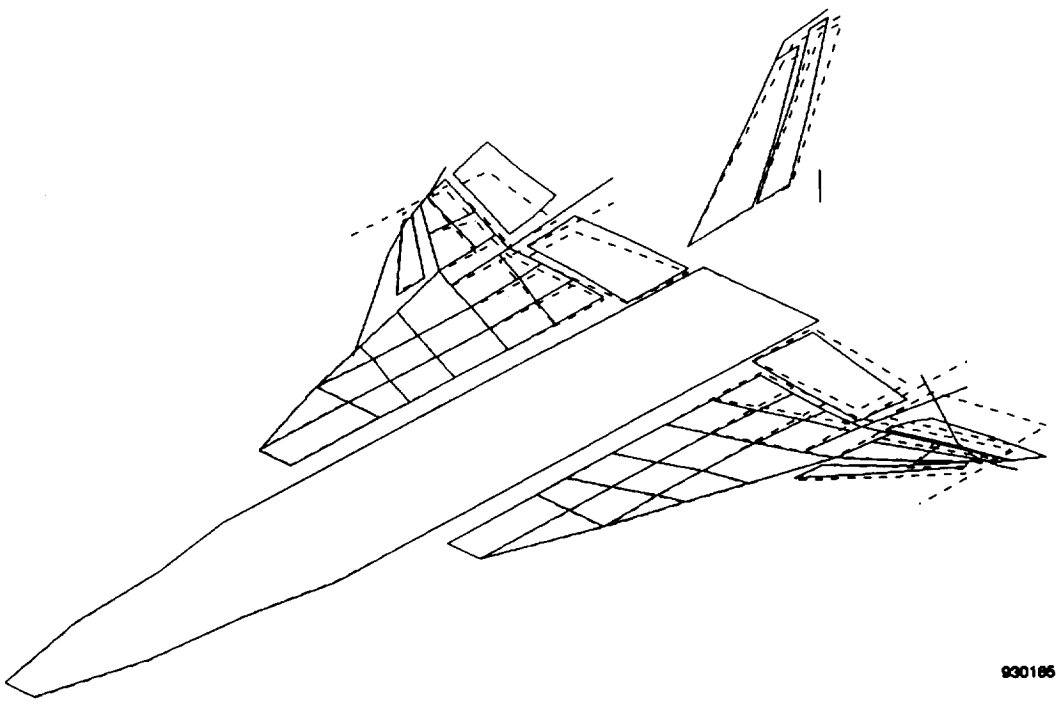

(a) Baseline, 13.24 Hz.

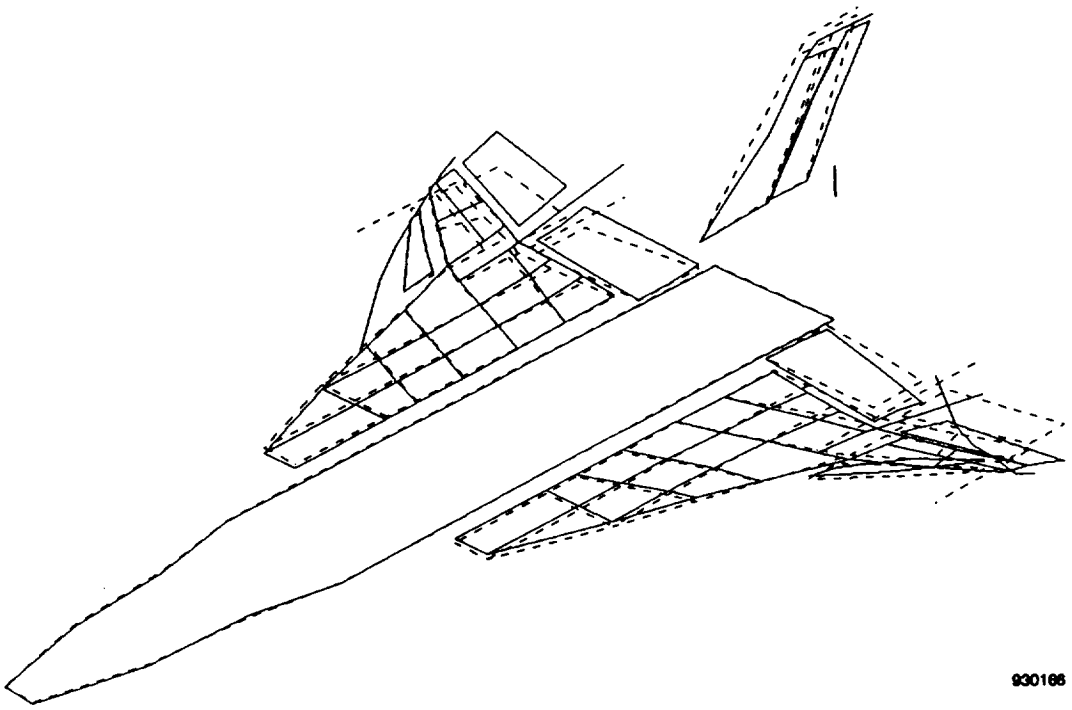

(b) Modified, 13.23 Hz.

Figure 19. Aircraft mode shapes, antisymmetric launcher rail bending.

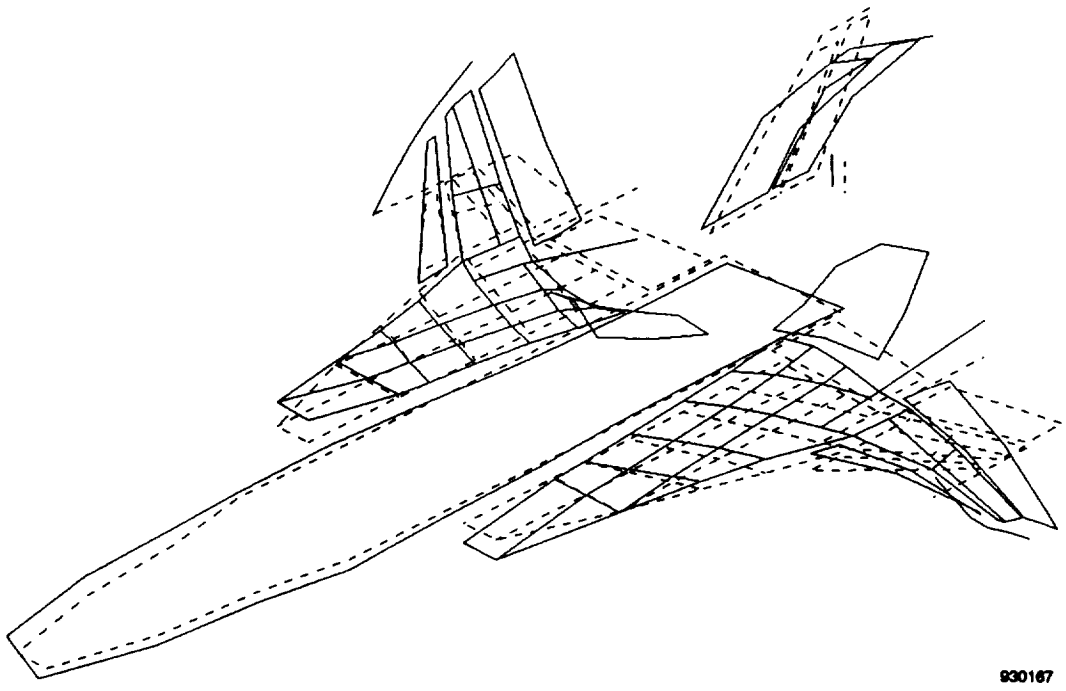

(a) Baseline, 20.36 Hz.

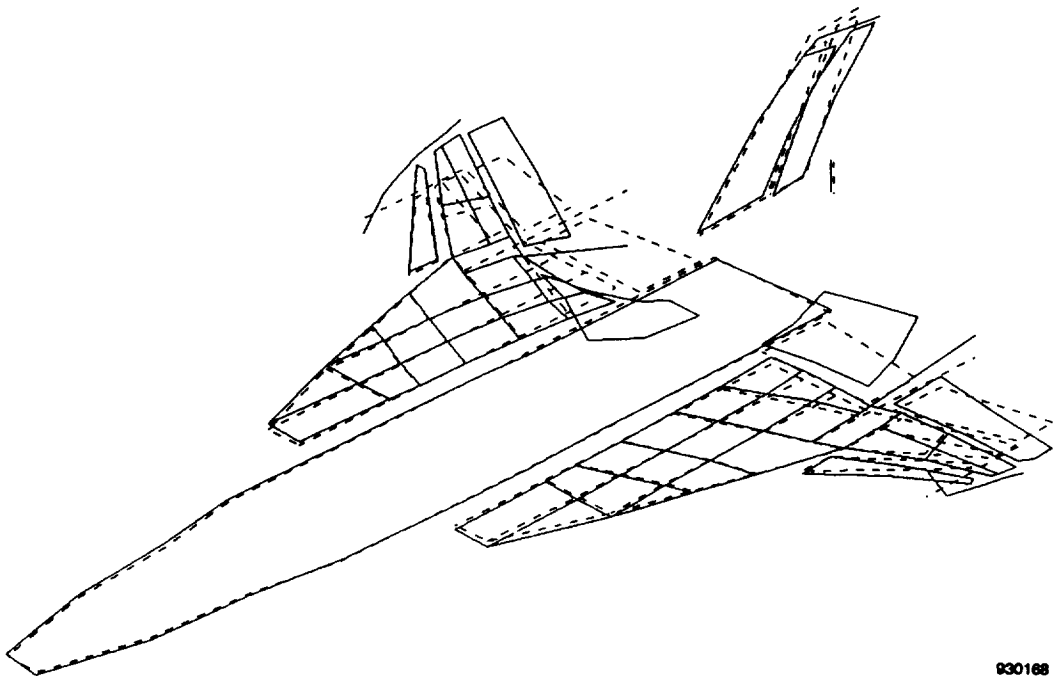

(b) Modified, 20.57 Hz.

Figure 20. Aircraft mode shapes, antisymmetric control surface mode 1.

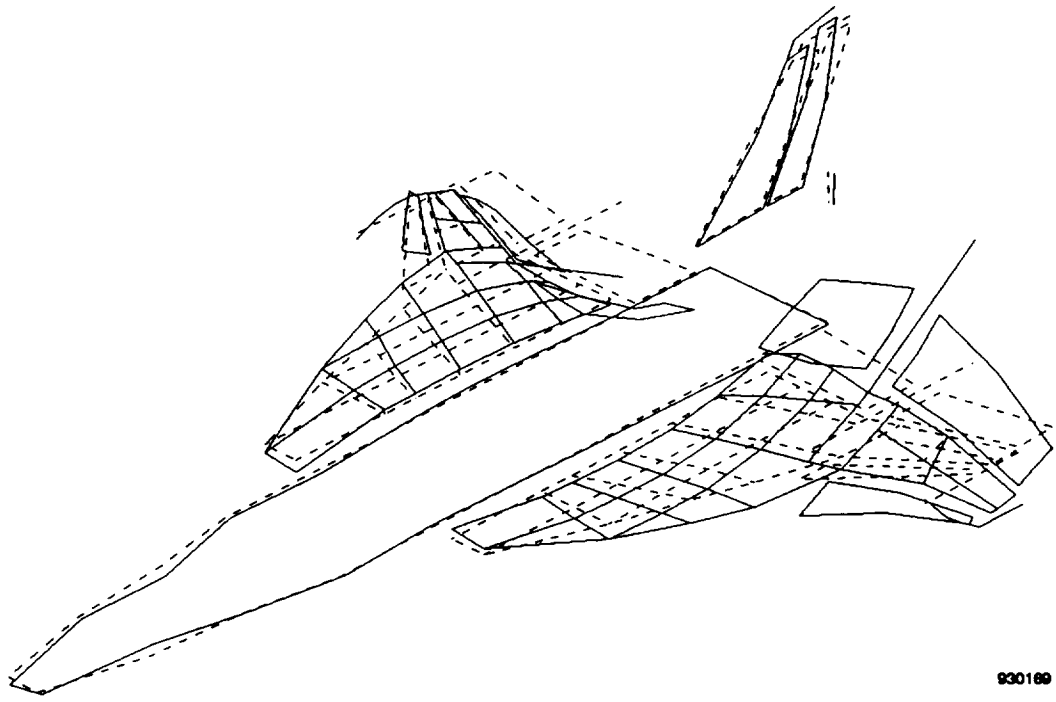

(a) Baseline, 22.19 Hz.

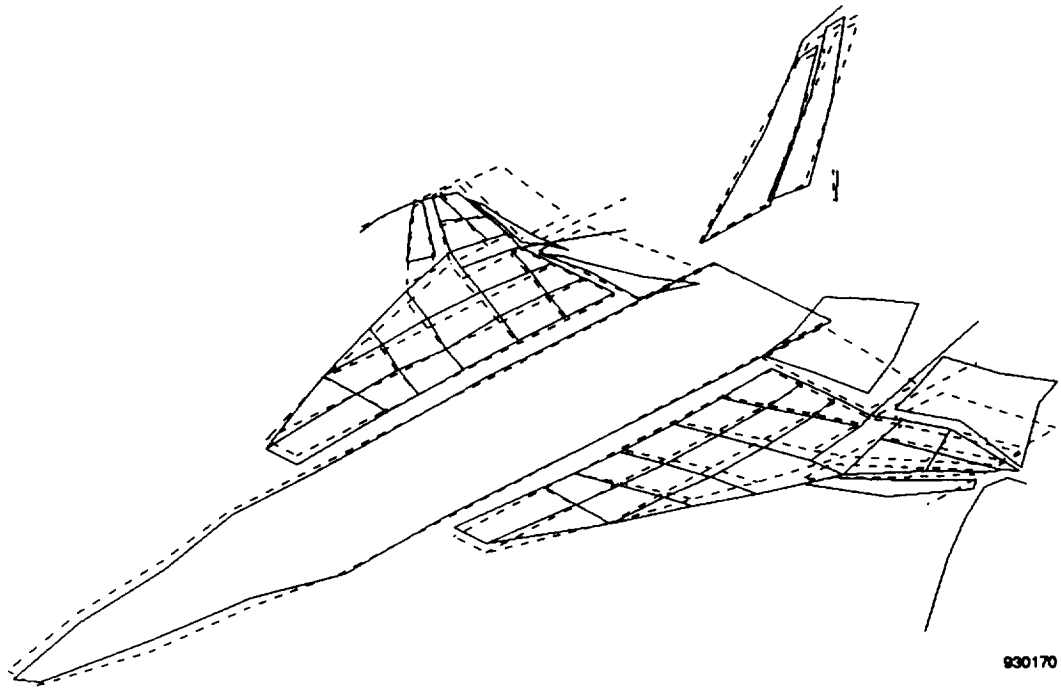

(b) Modified, 23.99 Hz.

Figure 21. Aircraft mode shapes, antisymmetric control surface mode 2.

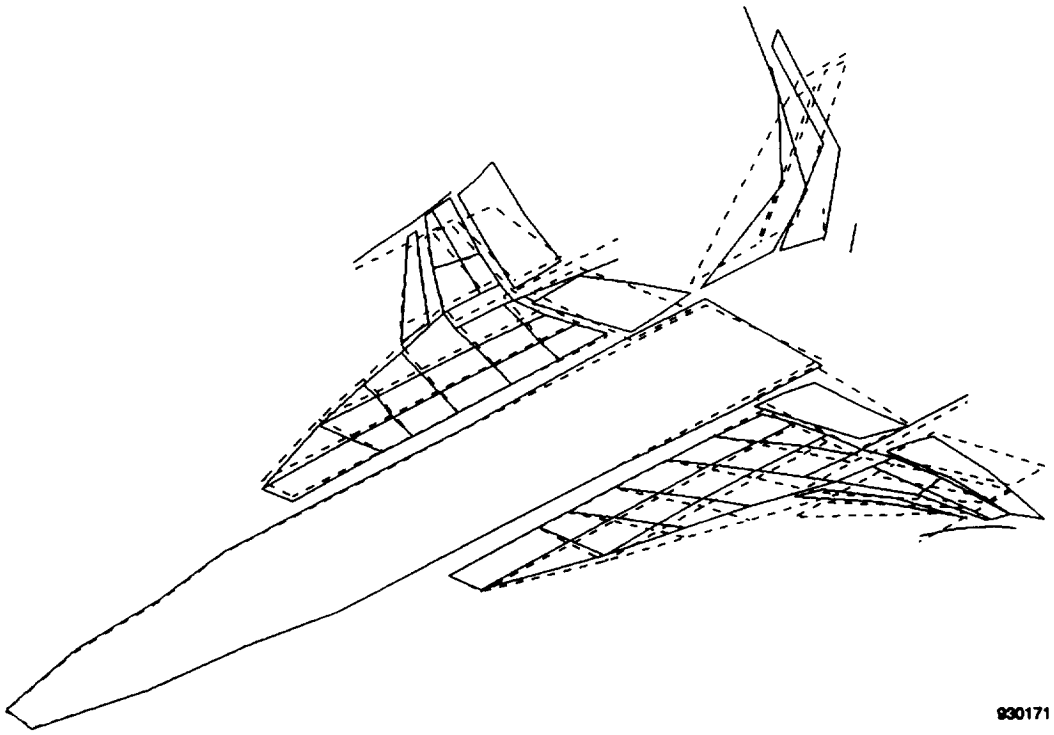

(a) Baseline, 27.05 Hz.

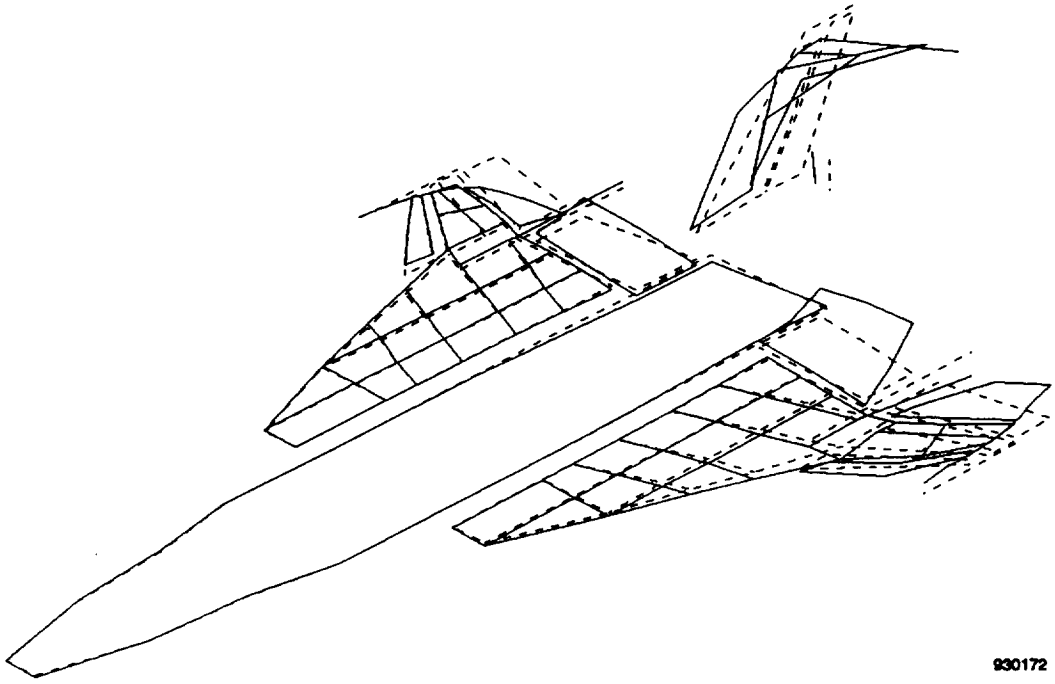

(b) Modified, 27.81 Hz.

Figure 22. Aircraft mode shapes, antisymmetric control surface mode 3.

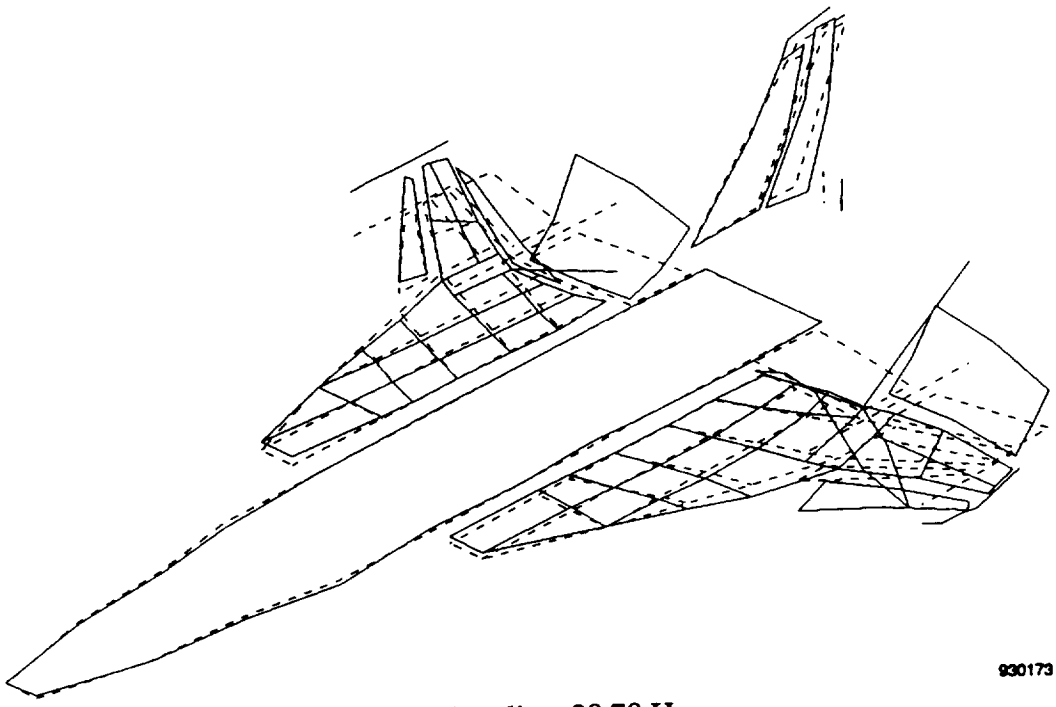

(a) Baseline, 28.78 Hz.

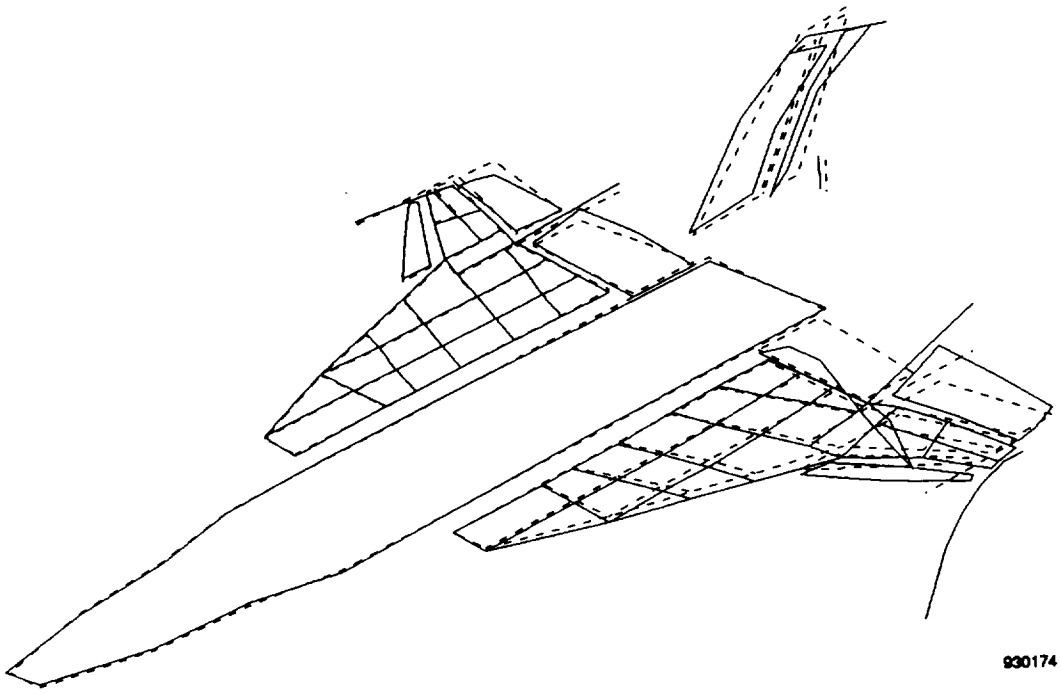

(b) Modified, 28.65 Hz.

Figure 23. Aircraft mode shapes, antisymmetric control surface mode 4.

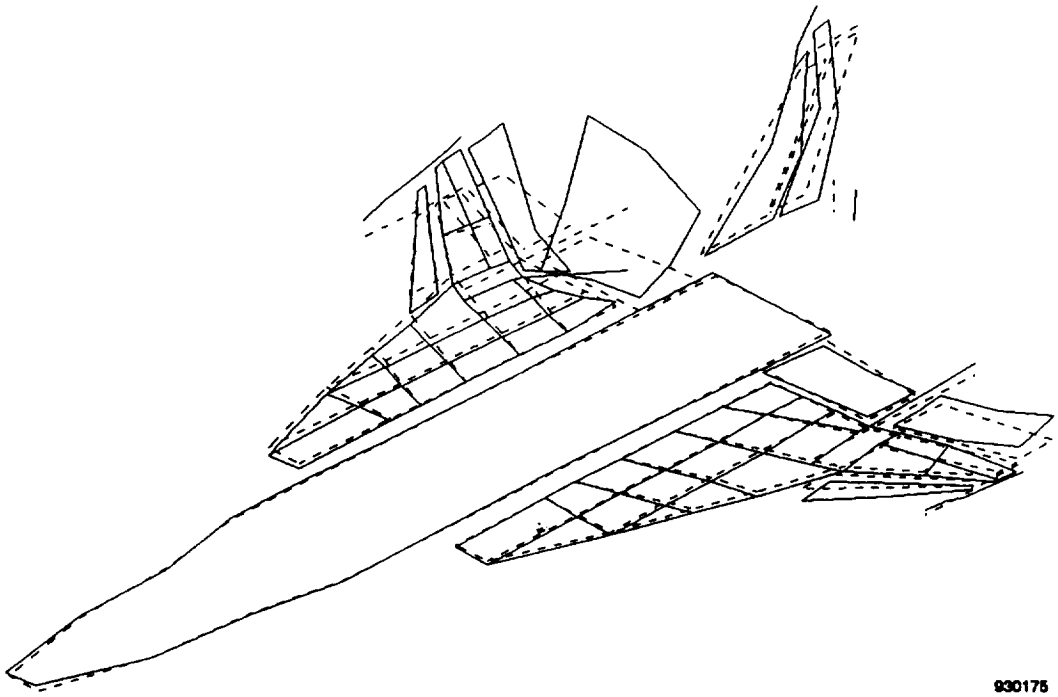

(a) Baseline, 27.17 Hz.

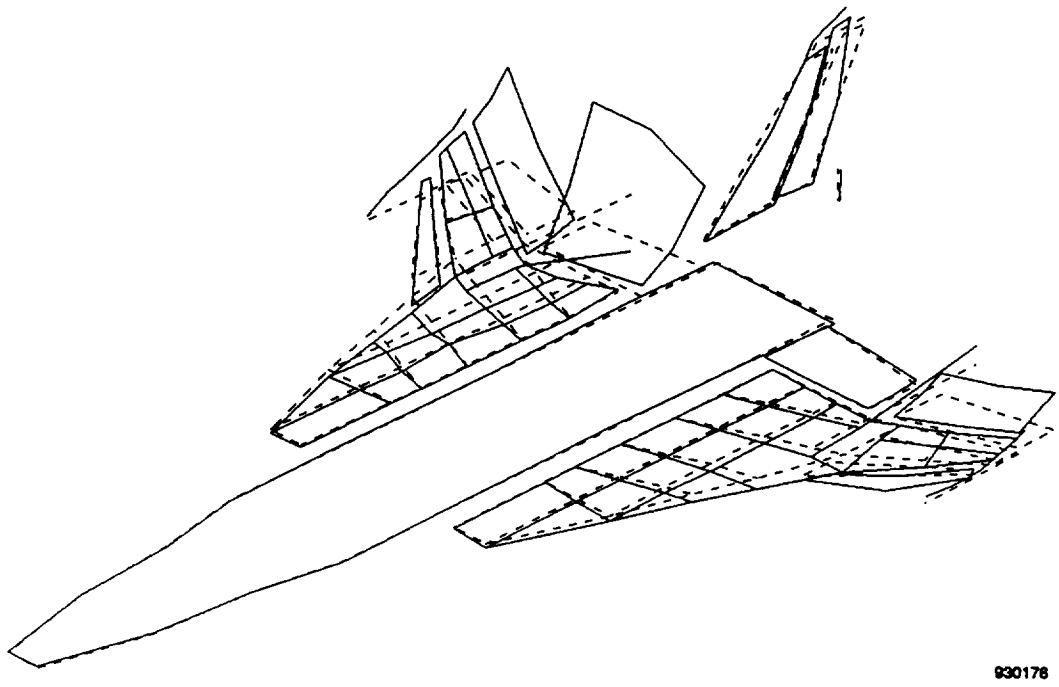

(b) Modified, 26.62 Hz.

Figure 24. Aircraft mode shapes, asymmetric control surface mode 1.

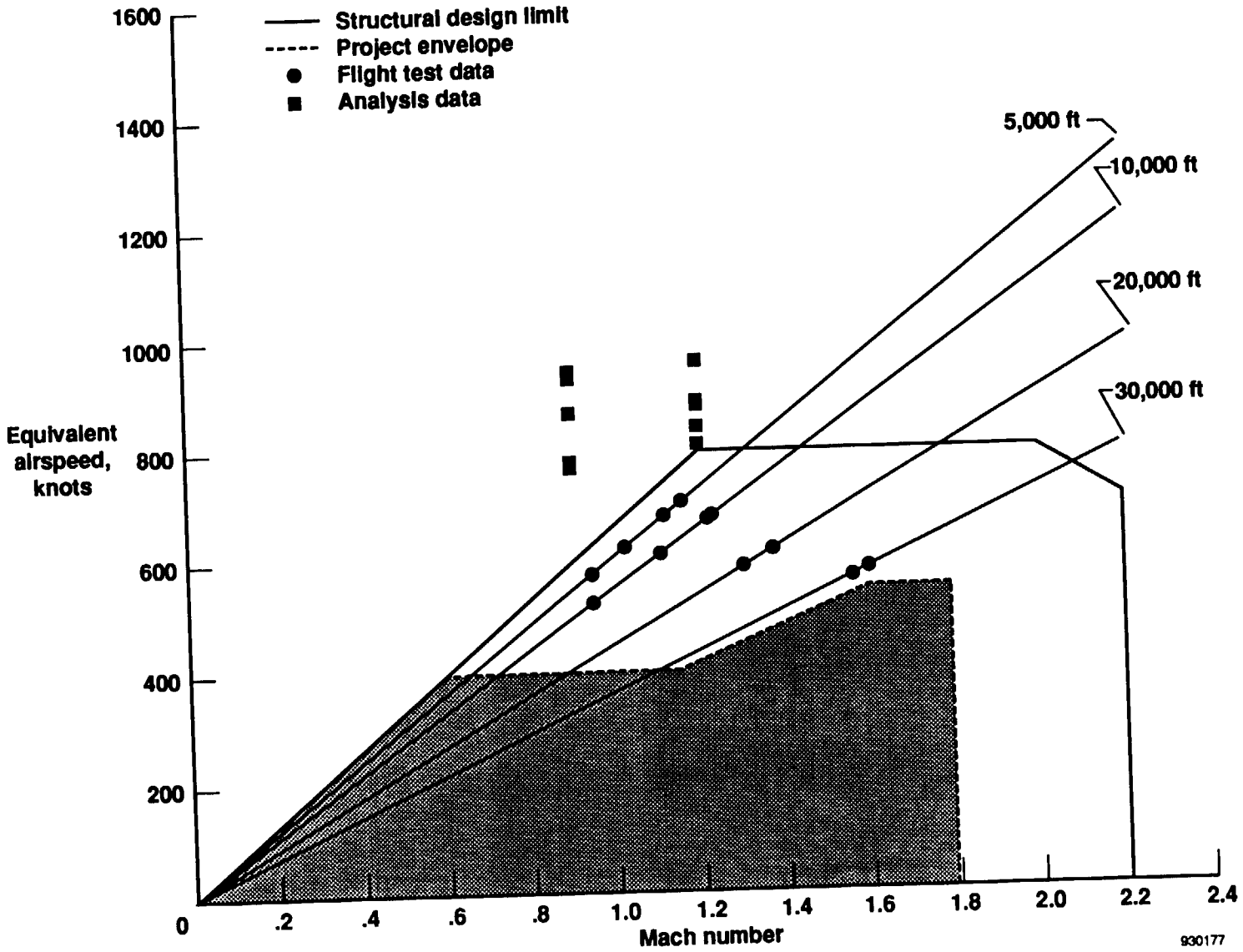

Figure 25. Summary of manufacturer's F-16XL flight and analysis test data.

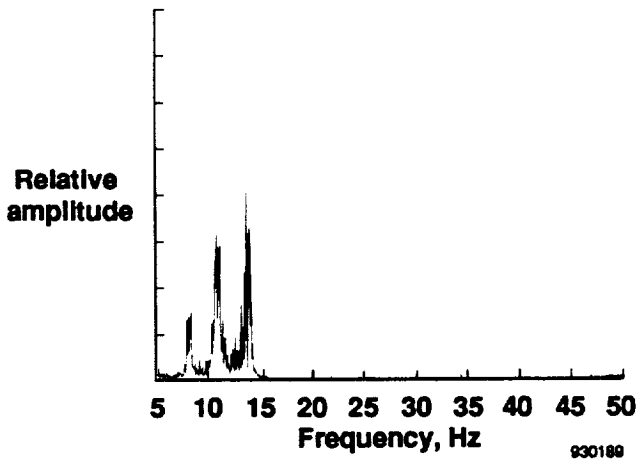

(a) 25,000 ft.

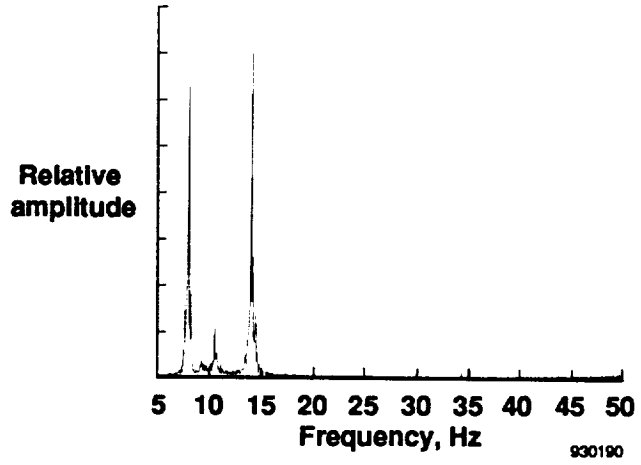

(b) 38,000 ft.

Figure 26 Left-wing forward accelerometer spectrum.

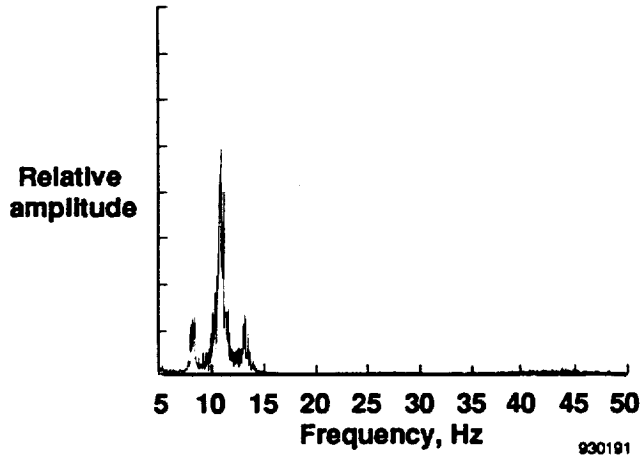

(a) 25,000 ft.

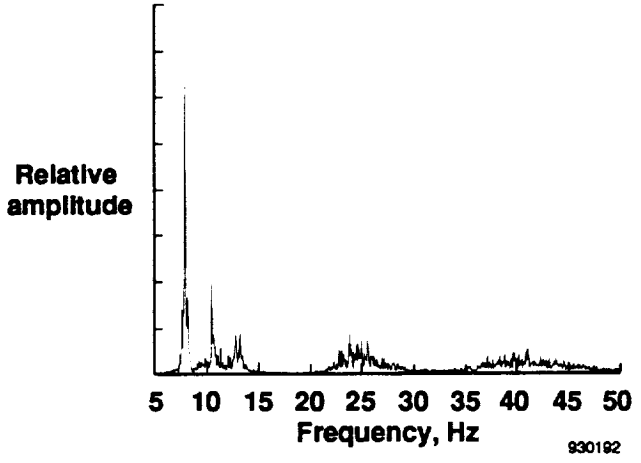

(b) 38,000 ft.

Figure 27. Right-wing forward accelerometer spectrum.

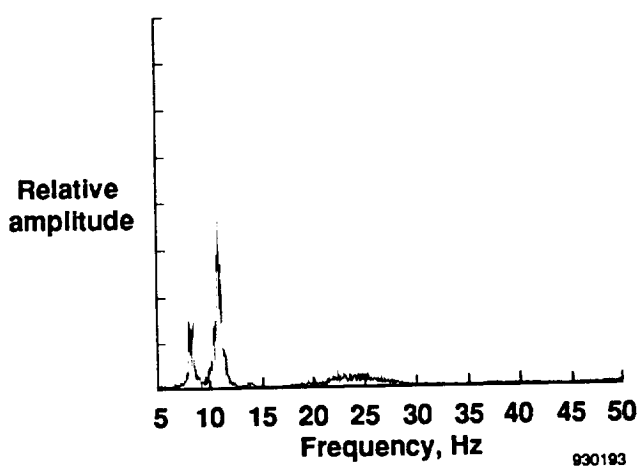

(a) 25,000 ft.

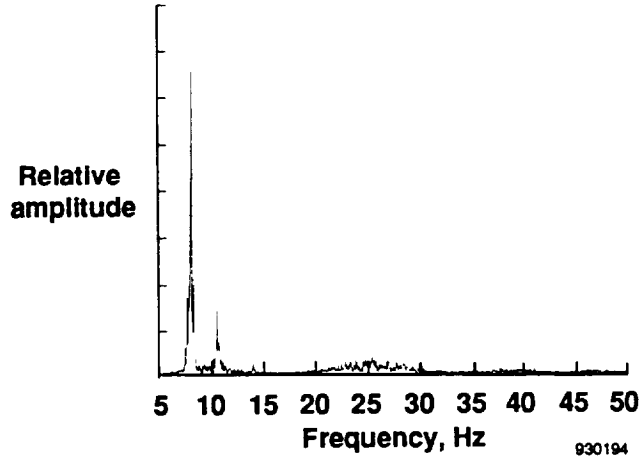

(b) 38,000 ft.

Figure 28. Left-wing aft accelerometer spectrum.

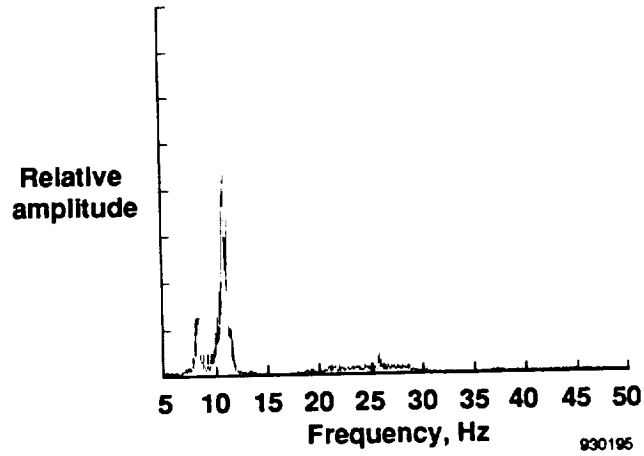

(a) 25,000 ft.

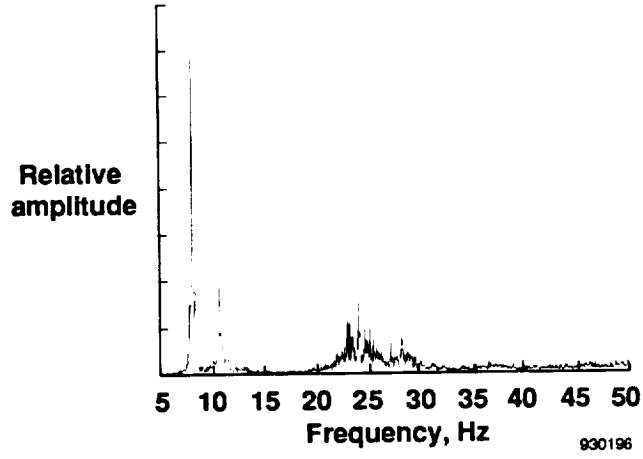

(b) 38,000 ft.

Figure 29. Right-wing aft accelerometer spectrum.

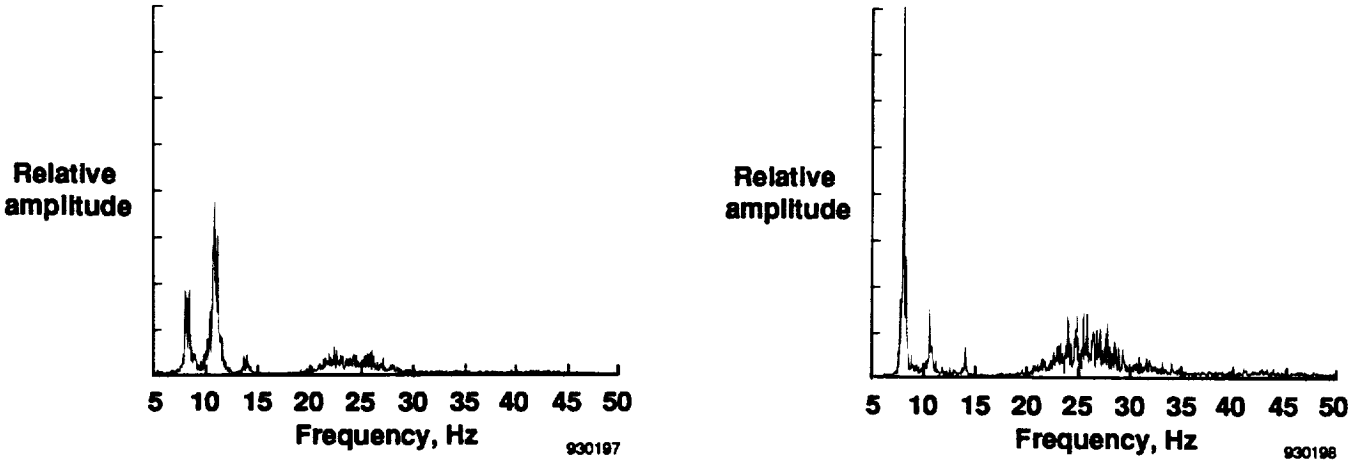

(a) 25,000 ft. (b) 38,000 ft.

Figure 30. Left-aileron beam accelerometer spectrum.

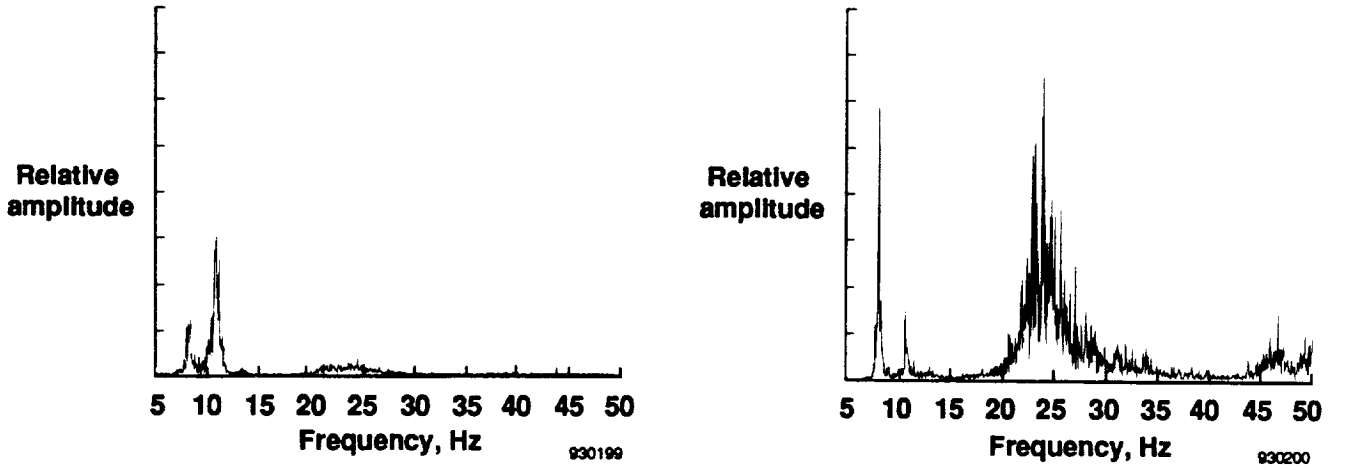

(a) 25,000 ft. (b) 38,000 ft.

Figure 31. Right-aileron beam accelerometer spectrum.

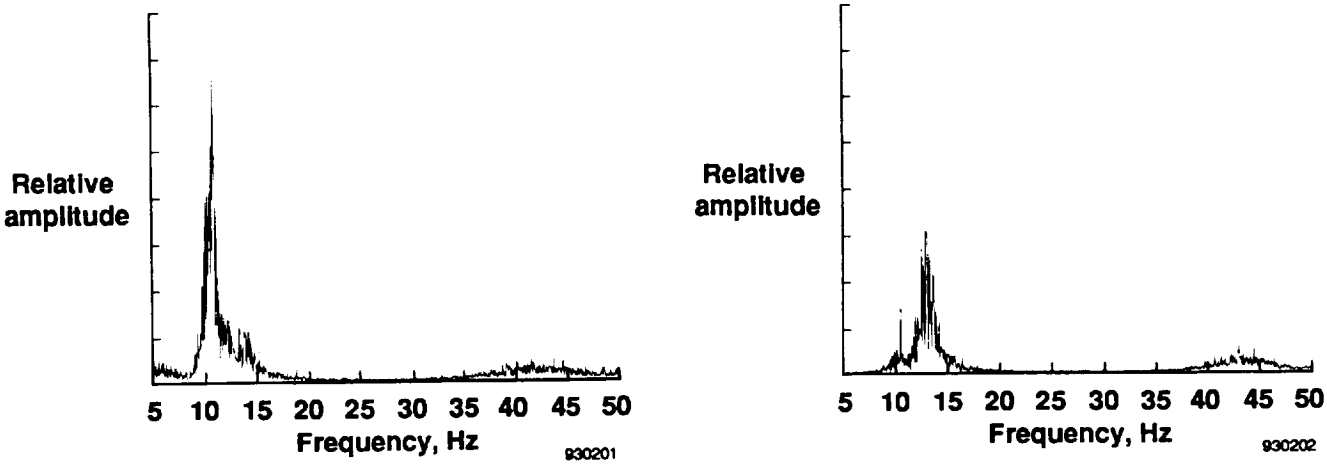

(a) 25,000 ft. (b) 38,000 ft.

Figure 32. Vertical-tail tip accelerometer spectrum.

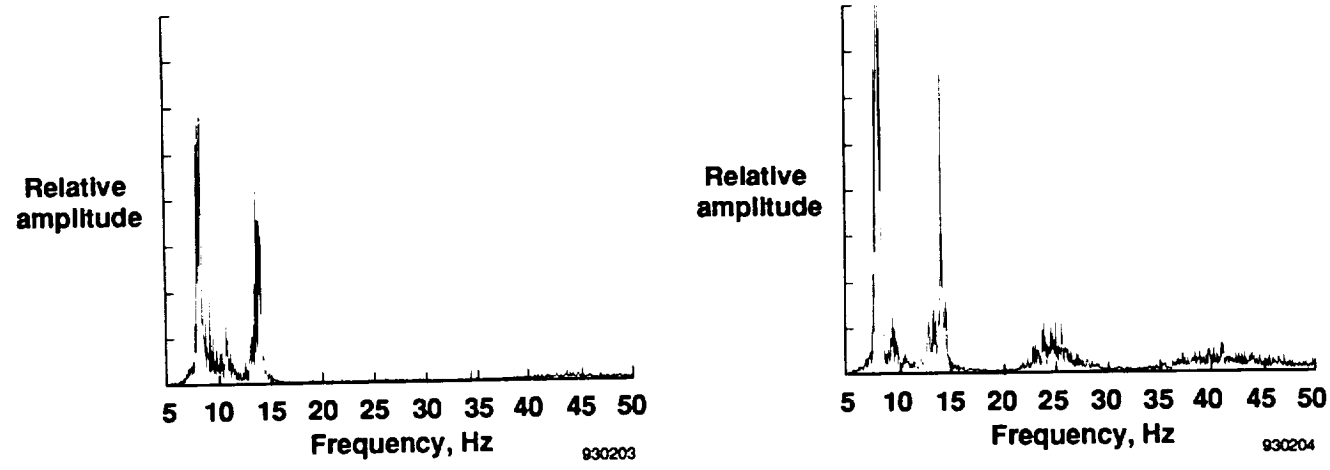

(a) 25,000 ft. (b) 38,000 ft.

Figure 33. Accelerometer spectrum for left- plus right-wing forward.

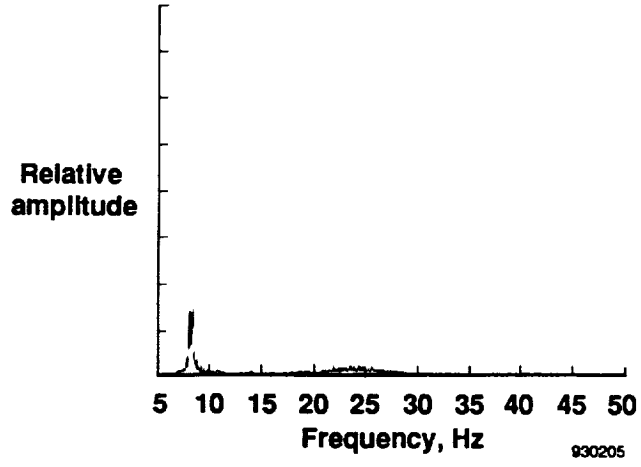

(a) 25,000 ft.

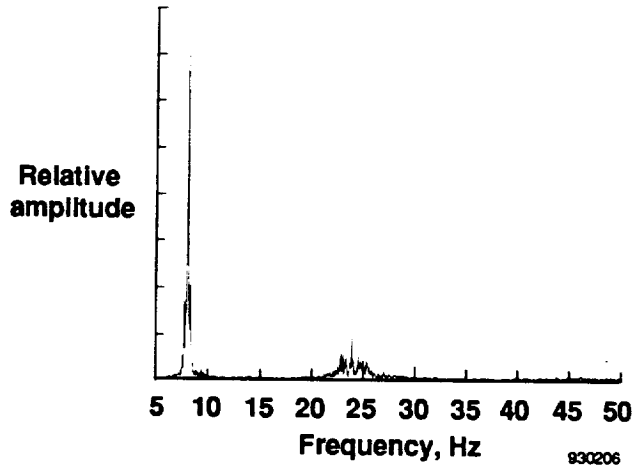

(b) 38,000 ft.

Figure 34. Accelerometer spectrum for left- plus right-wing aft.

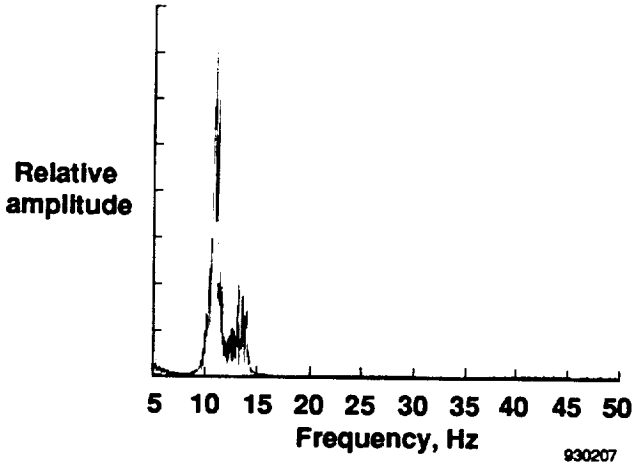

(a) 25,000 ft.

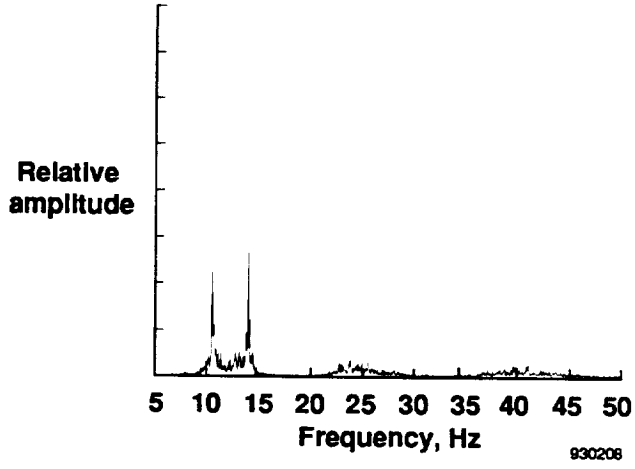

(b) 38,000 ft.

Figure 35. Accelerometer spectrum for left- minus right-wing forward.

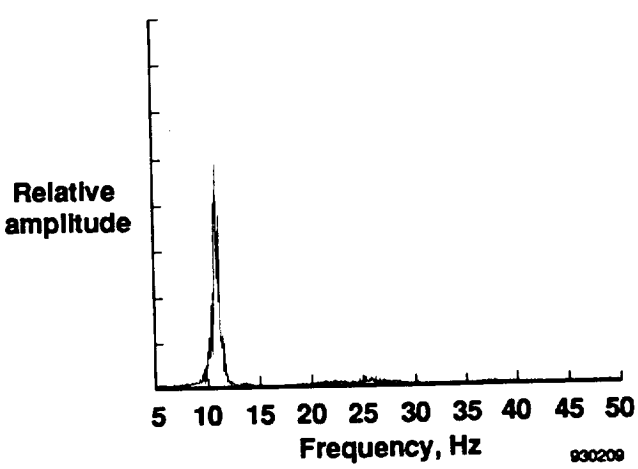

(a) 25,000 ft.

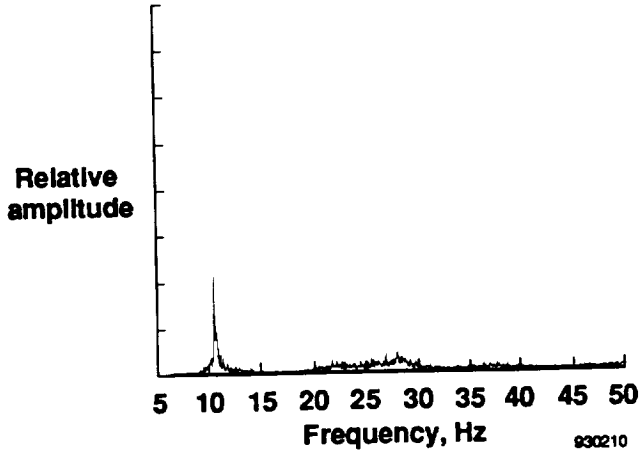

(b) 38,000 ft.

Figure 36. Accelerometer spectrum for left- minus right-wing aft.

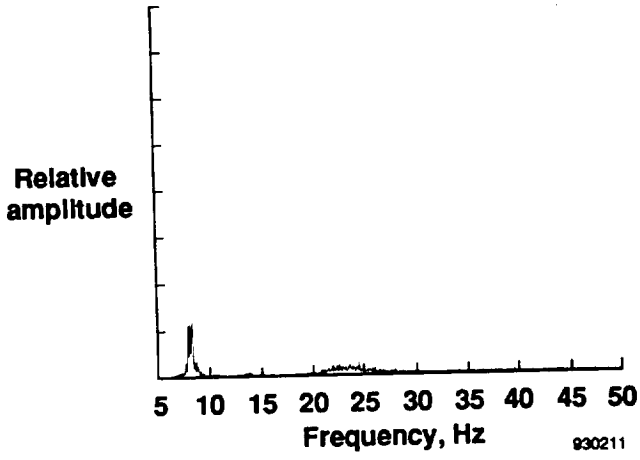

(a) 25,000 ft.

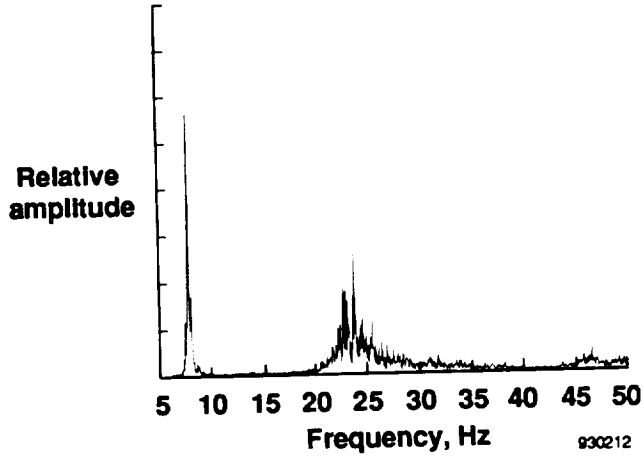

(b) 38,000 ft.

Figure 37. Accelerometer spectrum for left- plus right-aileron beam.

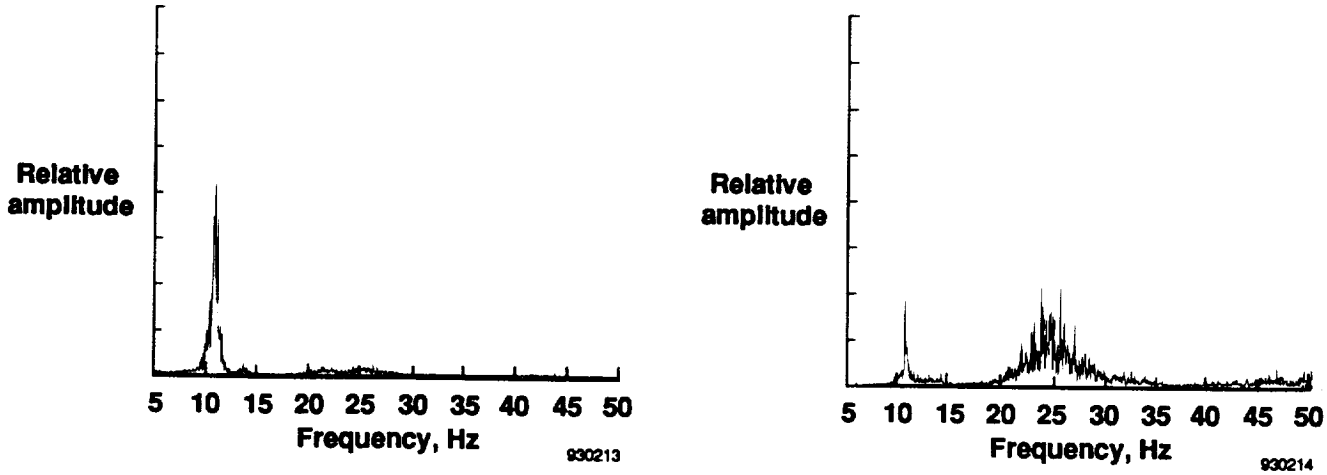

(a) 25,000 ft.

(b) 38,000 ft.

Figure 38. Accelerometer spectrum for left- plus right-aileron beam.

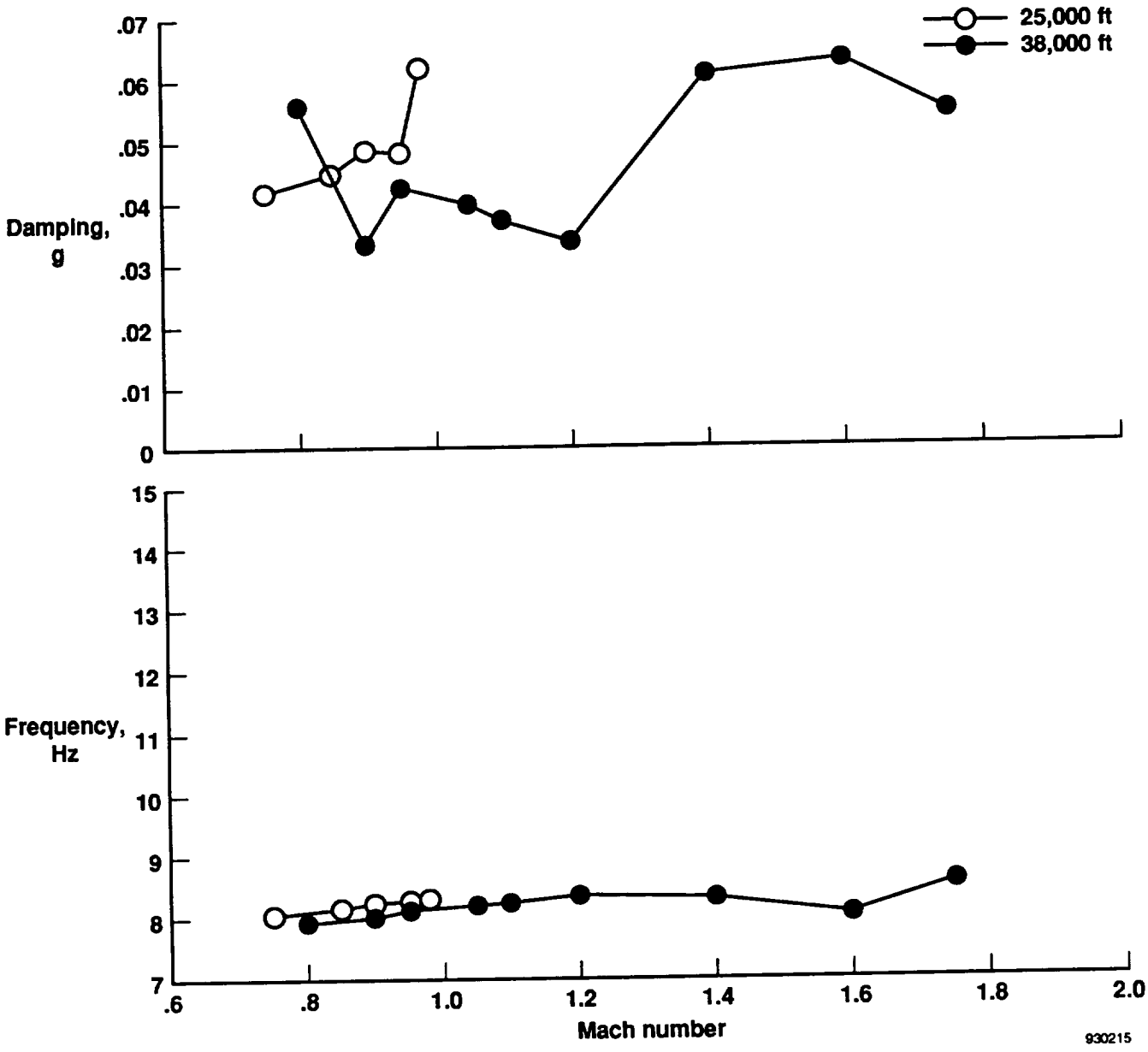

Figure 39. Symmetric wing bending flight test data.

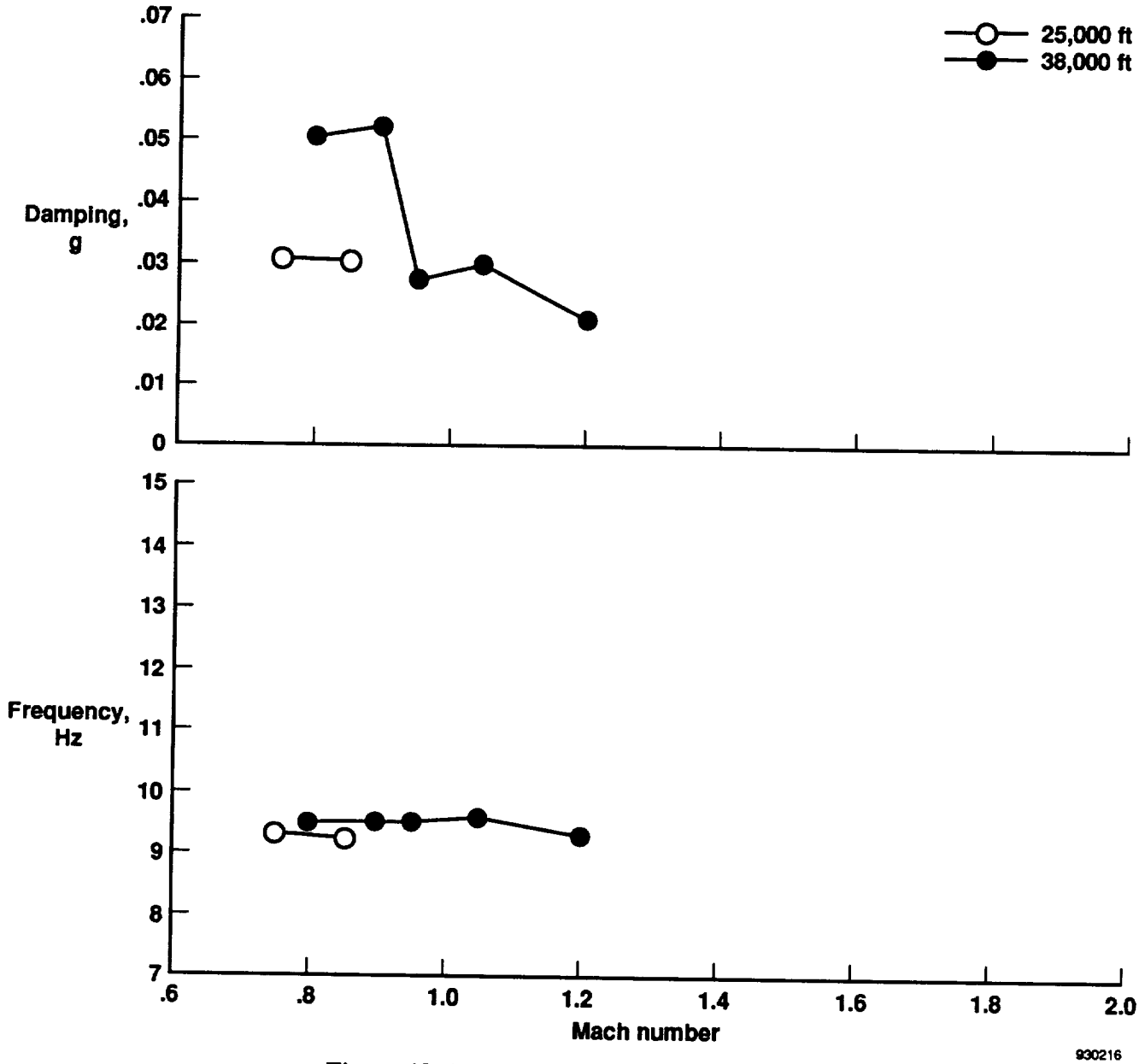

Figure 40. Fuselage bending flight test data.

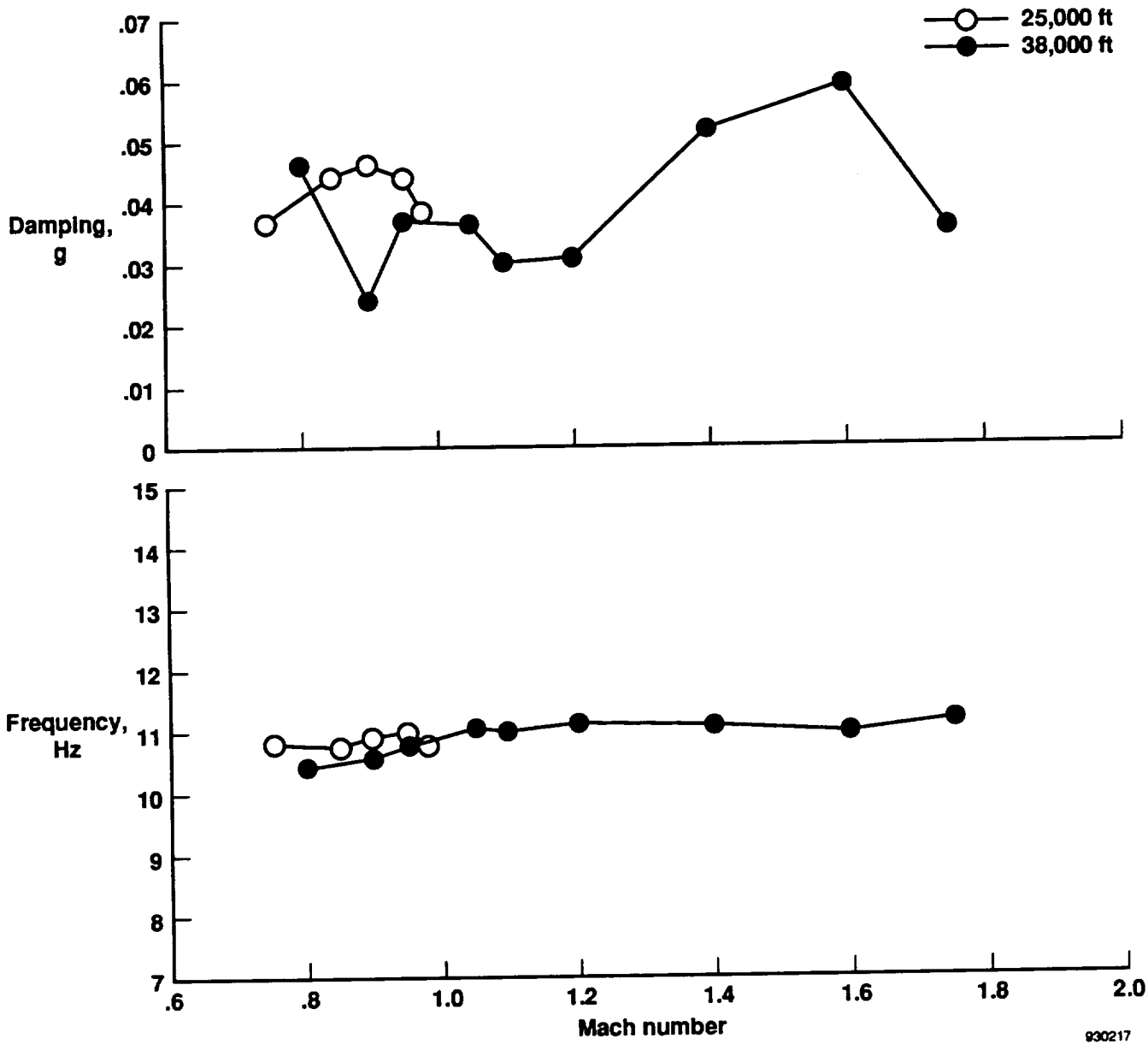

Figure 41. Antisymmetric wing bending flight test data.

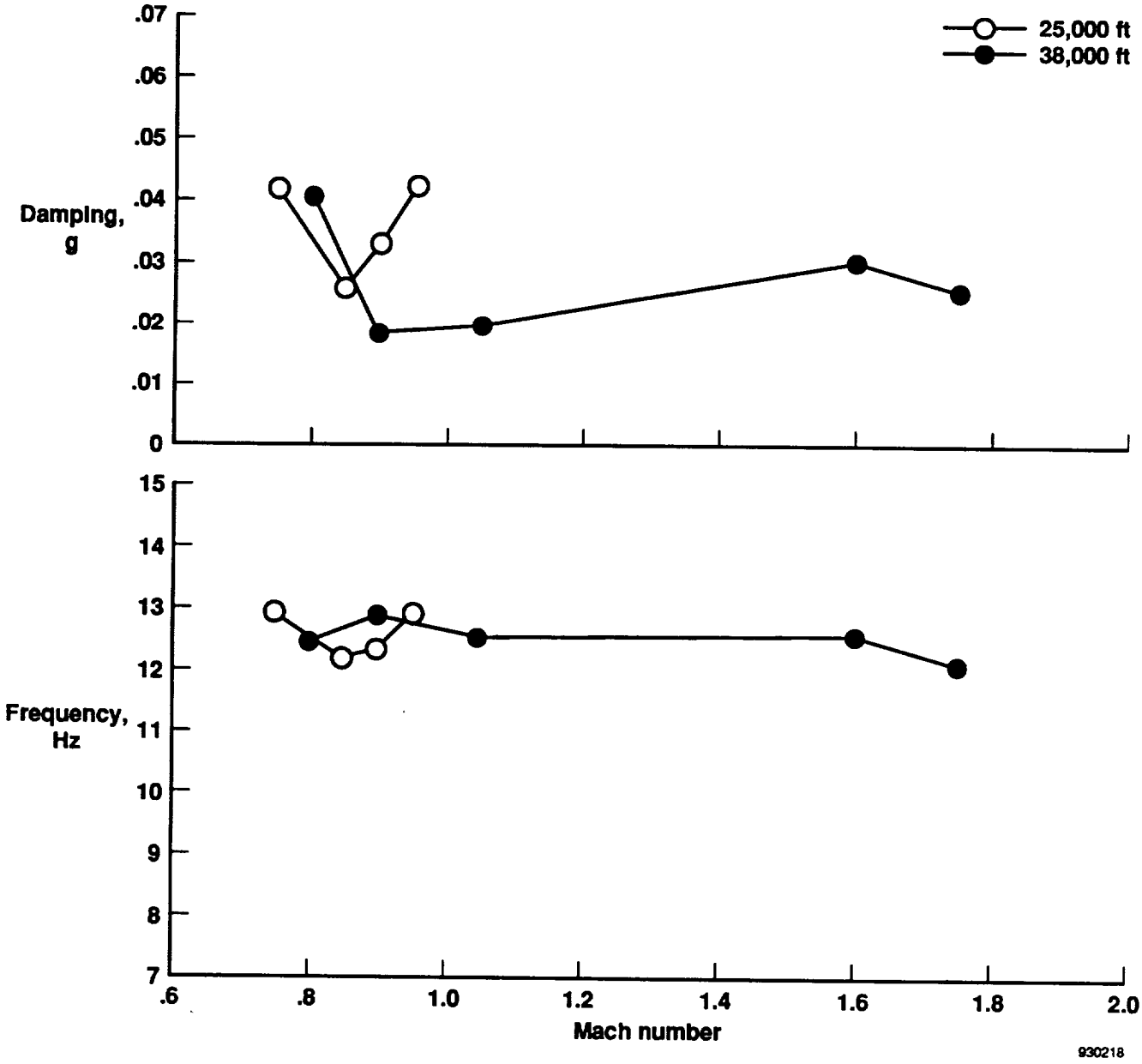

Figure 42. Vertical-tail bending flight test data.

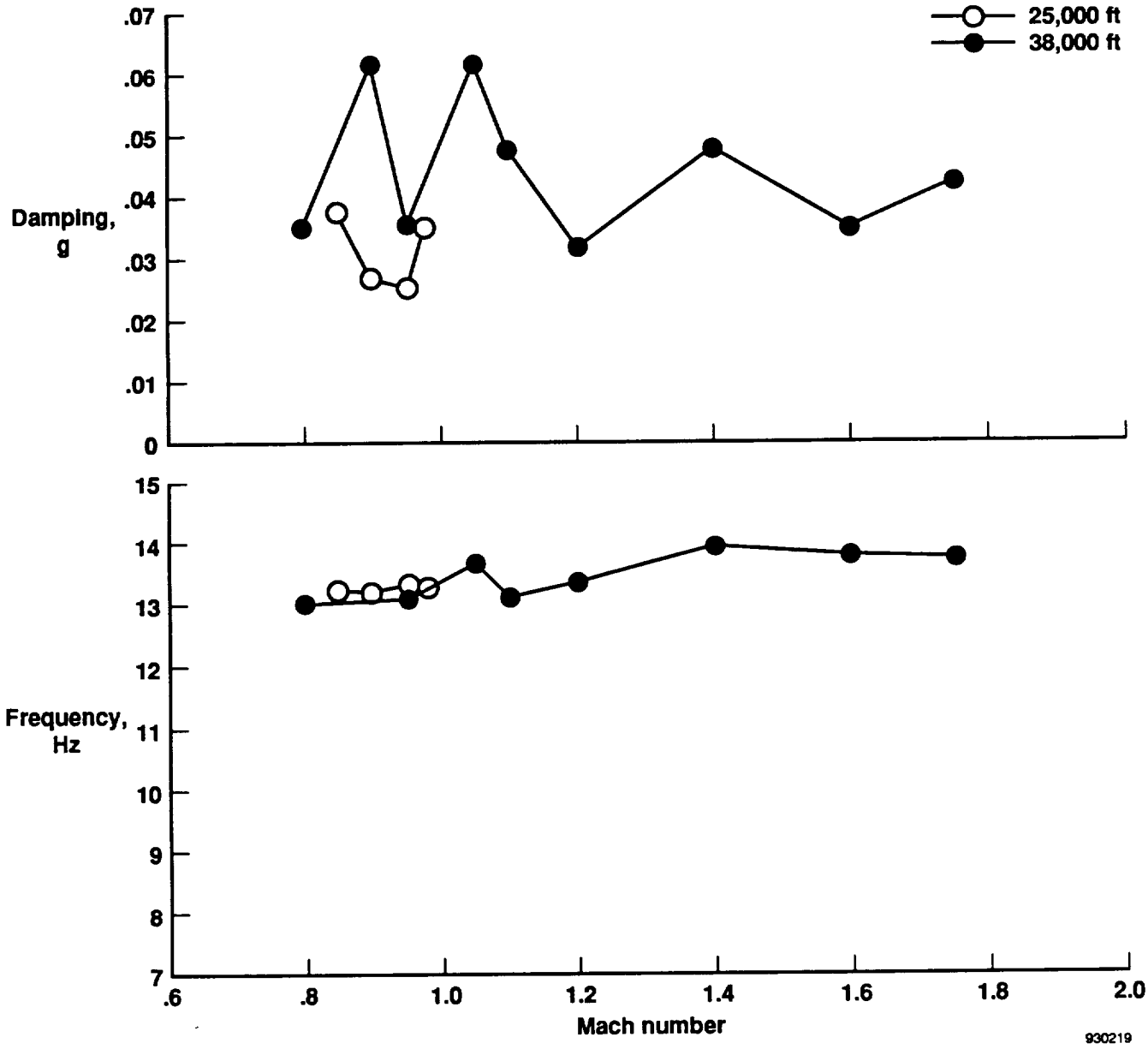

Figure 43. Antisymmetric launcher bending flight test data.

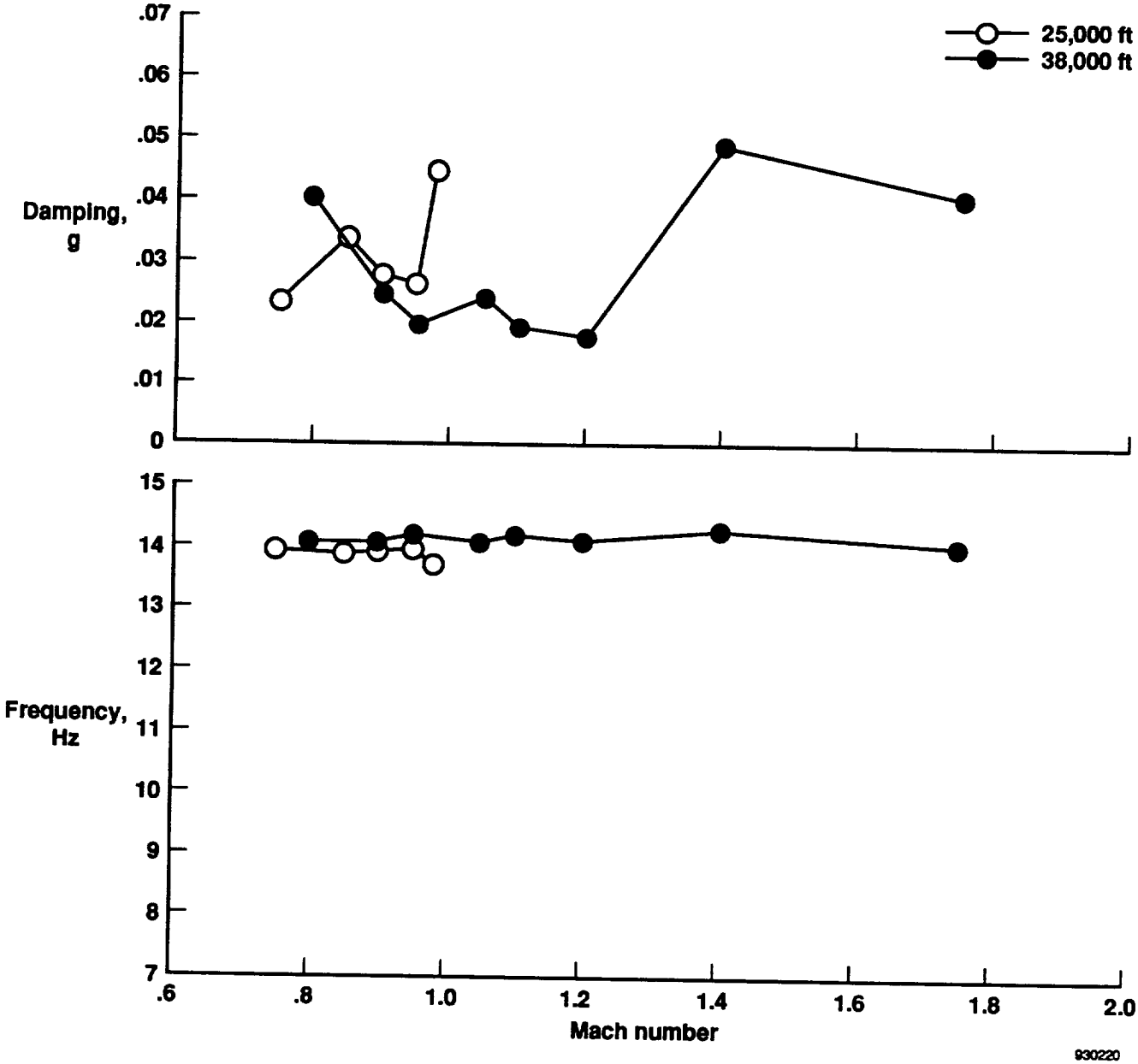

Figure 44. Symmetric launcher bending flight test data.

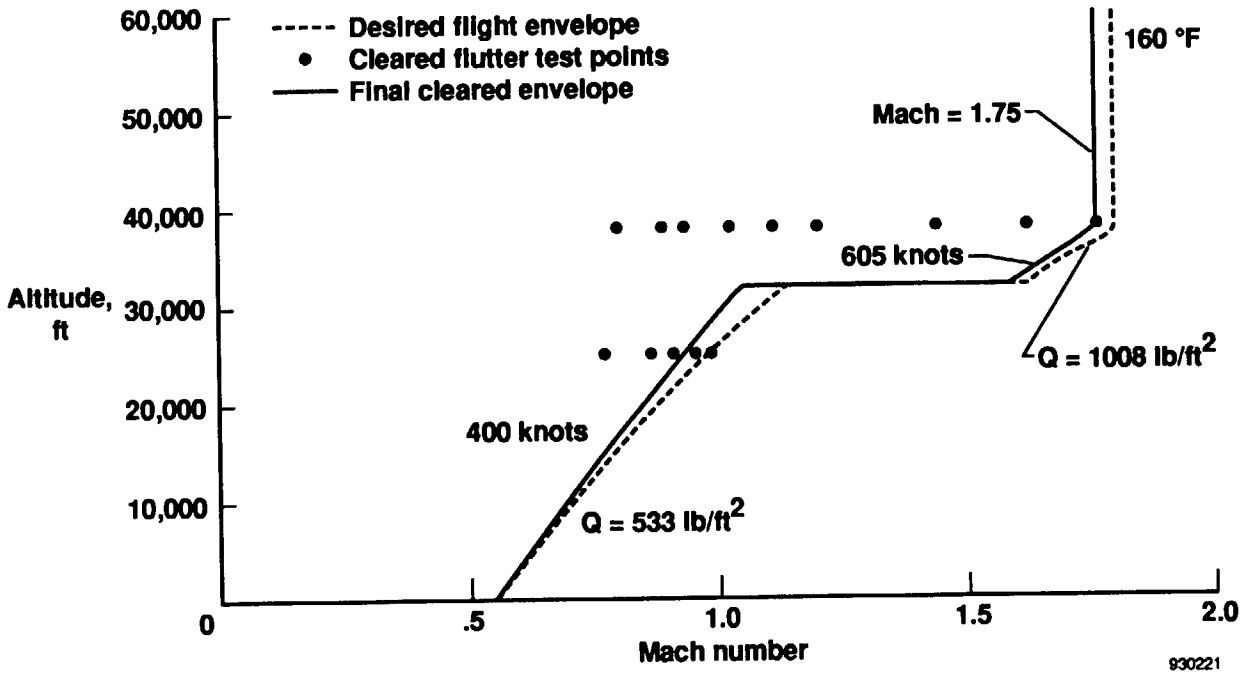

Figure 45. Final cleared flutter envelope.

APPENDIX

Table A-1. F-16XL accelerometer locations for GVT.

Point number	Fuselage station	Span location	Waterline
101	475	−194	91
102	480	−194	91
103	493	−194	91
104	461	−193	91
105	497	−192	91
106	509	−192	91
107	522	−192	91
108	465	−191	91
109	454	−168	91
110	430	−165	91
111	442	−164	91
112	486	−161	91
113	515	−161	91
114	480	−160	91
115	400	−137	91
116	420	−137	91
117	430	−136	91
118	456	−136	91
119	471	−136	91
120	491	−129	91
121	508	−129	91
122	474	−129	91
123	386	−123	91

Table A-1. Continued.

Point number	Fuselage station	Span location	Waterline
124	423	–121	91
125	458	–121	91
126	465	–121	91
127	542	–121	91
128	471	–114	91
129	489	–114	91
130	506	–114	91
131	349	–112	91
132	305	–99	91
133	344	–98	91
134	376	–98	91
135	414	–98	91
136	449	–98	91
137	465	–98	91
138	471	–78	91
139	511	–78	91
140	243	–76	91
141	305	–76	91
142	335	–76	91
143	367	–76	91
144	405	–76	91
145	439	–76	91
146	465	–76	91
147	243	–54	91
148	305	–54	91
149	326	–54	91
150	359	–54	91
151	396	–54	91

Table A-1. Continued.

Point number	Fuselage station	Span location	Waterline
152	430	–54	91
153	465	–54	91
154	471	–43	91
155	493	–43	91
156	515	–43	91
157	425	–196	91
158	440	–196	91
159	452	–196	91
160	465	–196	91
161	482	–196	91
162	496	–196	91
201	475	194	91
202	480	194	91
203	493	194	91
204	461	193	91
205	497	192	91
206	509	192	91
207	522	192	91
208	465	191	91
209	454	168	91
210	430	165	91
211	442	164	91
212	486	161	91
213	515	161	91
214	480	160	91
215	400	137	91
216	420	137	91
217	430	136	91

Table A-1. Continued.

Point number	Fuselage station	Span location	Waterline
218	456	136	91
219	471	136	91
220	491	129	91
221	508	129	91
222	474	129	91
223	386	123	91
224	423	121	91
225	458	121	91
226	565	121	91
227	542	121	91
228	471	114	91
229	489	114	91
230	506	114	91
231	349	112	91
232	305	99	91
233	344	98	91
234	376	98	91
235	414	98	91
236	449	98	91
237	465	98	91
238	471	78	91
239	511	78	91
240	243	76	91
241	305	76	91
242	334	76	91
243	367	76	91
244	405	76	91
245	439	76	91

Table A-1. Continued.

Point number	Fuselage station	Span location	Waterline
246	465	76	91
247	243	54	91
248	305	54	91
249	326	54	91
250	358	54	91
251	396	54	91
252	430	54	91
253	465	54	91
254	471	43	91
255	493	43	91
256	515	43	91
257	425	196	91
258	440	196	91
259	452	196	91
260	465	196	91
261	482	196	91
262	496	196	91
301	548	0	225
302	584	0	227
303	540	0	217
304	560	0	217
305	568	0	223
306	583	0	223
307	513	0	188
308	536	0	174
309	551	0	194
310	565	0	185
311	470	0	141

Table A-1. Continued.

Point number	Fuselage station	Span location	Waterline
312	518	0	144
313	521	0	144
314	546	0	145
315	567	0	127
316	567	0	145
401	10	–10	91
402	10	–10	91
403	10	10	91
404	10	10	91
405	70	–25	91
406	70	–25	91
407	70	25	91
408	70	25	91
409	130	–30	91
410	130	–30	91
411	130	30	91
412	130	30	91
413	182	–40	91
414	182	–40	91
415	182	40	91
416	182	40	91
417	243	–40	91
418	243	–40	91
419	243	40	91
420	243	40	91
421	310	–40	91
422	310	–40	91
423	310	40	91

Table A-1. Concluded.

Point number	Fuselage station	Span location	Waterline
424	310	40	91
425	385	–40	91
426	385	–40	91
427	385	40	91
428	385	40	91
429	465	–40	91
430	465	–40	91
431	465	40	91
432	465	40	91
433	524	–40	91
434	524	–40	91
435	524	40	91
436	524	40	91
437	558	–40	91
438	558	–40	91
439	558	40	91
440	558	40	91

Shaker/force transducer locations

Shaker no.	Driving point accelerometer	Fuselage station	Span location	Waterline
1	157	425	-196	91
2	262	482	196	91
3	303	540	0	217

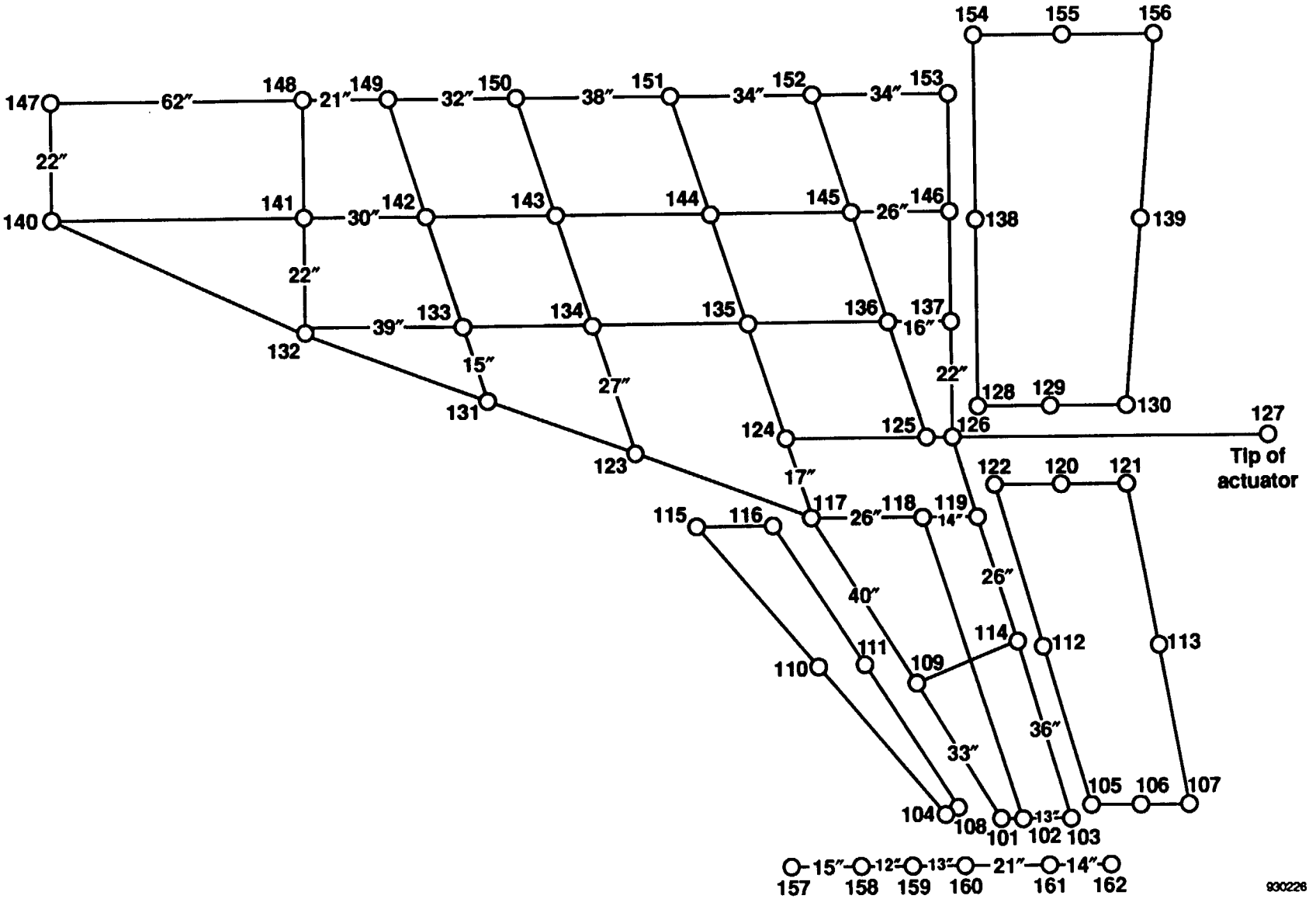
154
155
156
147
62″
148
21″
149
32″
150
38″
151
34″
152
34″
153
22″
140
141
30″
142
143
144
145
26″
146
138
139
22″
132
39″
133
134
135
136
137
16″
15″
131
27″
22″
128
129
130
127
Tip of actuator
124
125
126
123
17″
122
120
121
115
116
117
26″
118
119
14″
26″
40″
114
112
113
111
109
110
36″
33″
105
106
107
104
108
101
102
103
15″
12″
13″
21″
14″
157
158
159
160
161
162
930226

Figure A-1.

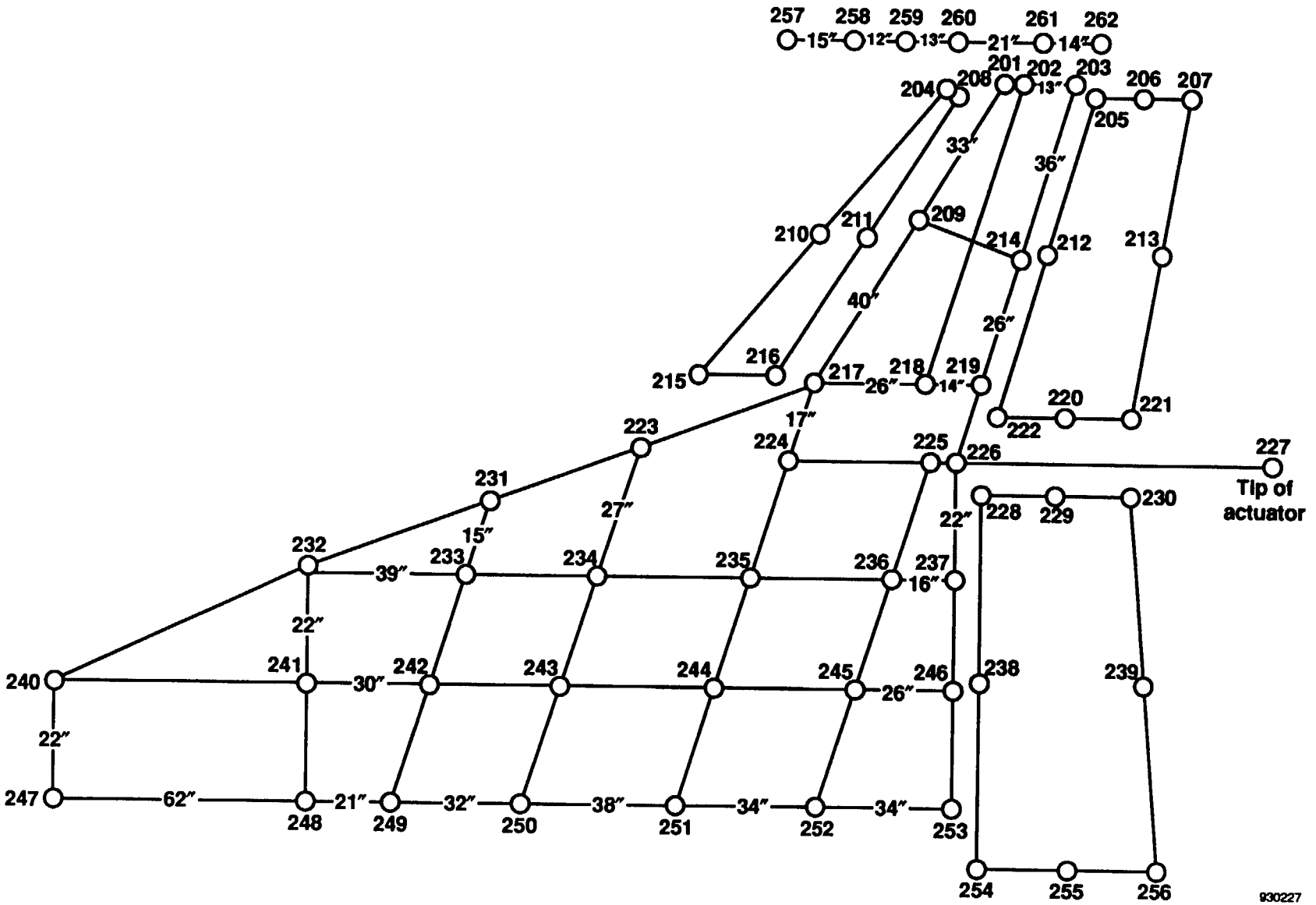
257
258
259
260
261
262
15″
12″
13″
21″
14″
201
202
203
204
208
13″
206
207
205
33″
36″
209
210
211
214
212
213
40″
26″
215
216
217
218
219
26″
14″
220
221
222
17″
223
224
225
226
227
Tip of actuator
231
27″
22″
228
229
230
15″
232
233
234
235
236
237
39″
16″
22″
241
242
243
244
245
246
238
239
240
30″
26″
22″
247
62″
248
21″
249
32″
250
38″
251
34″
252
34″
253
254
255
256
930227

Figure A-2.

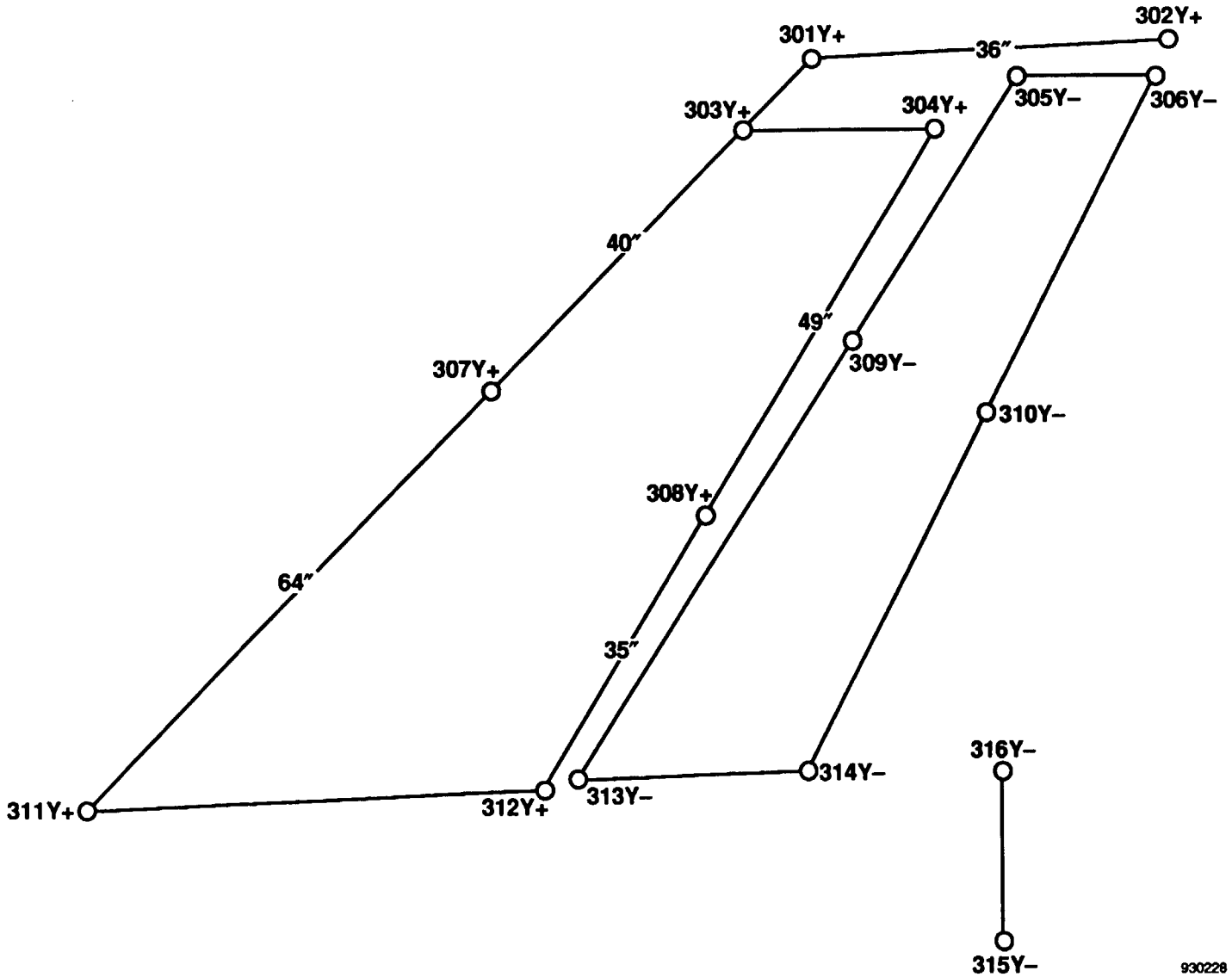
301Y+
302Y+
36″
303Y+
304Y+
305Y–
306Y–
40″
49″
307Y+
309Y–
310Y–
308Y+
64″
35″
311Y+
312Y+
313Y–
314Y–
316Y–
315Y–
930228

Figure A-3.

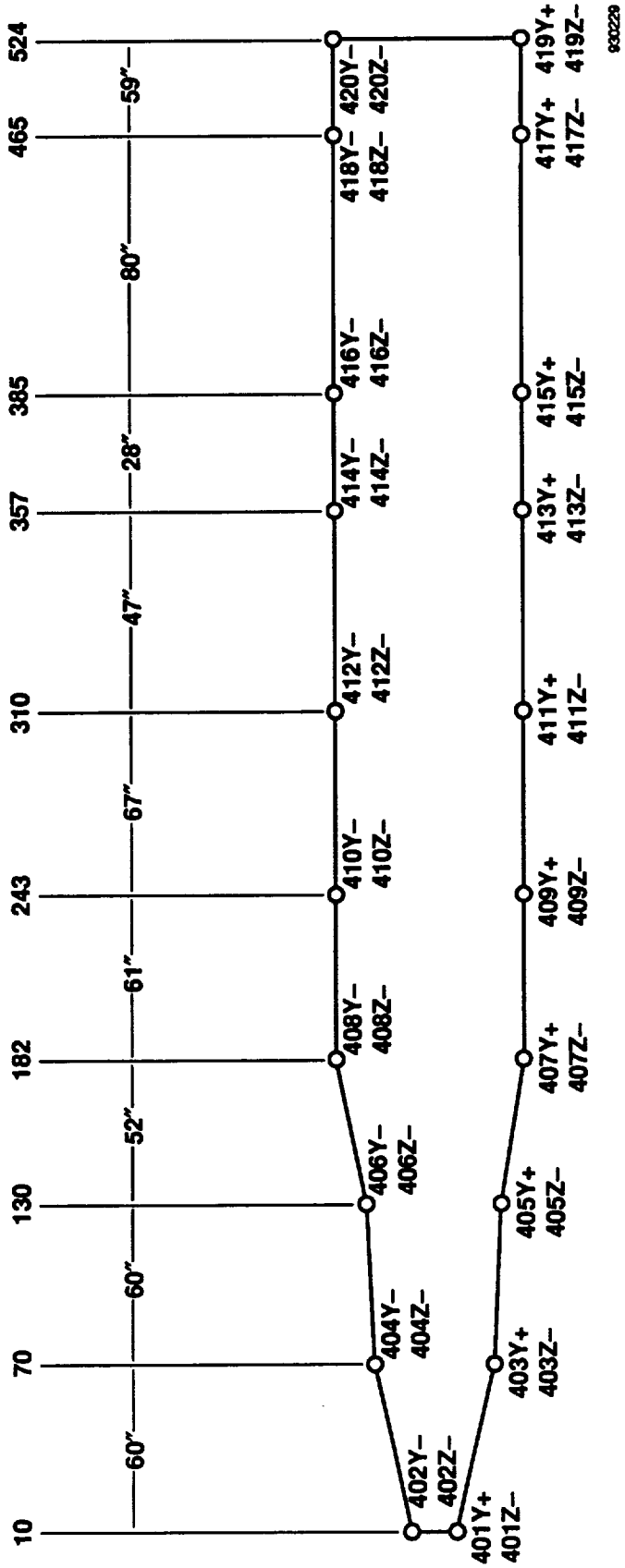
10
70
130
182
243
310
357
385
465
524
60″
60″
52″
61″
67″
47″
28″
80″
59″
401Y+
401Z–
402Y–
402Z–
403Y+
403Z–
404Y–
404Z–
405Y+
405Z–
406Y–
406Z–
407Y+
407Z–
408Y–
408Z–
409Y+
409Z–
410Y–
410Z–
411Y+
411Z–
412Y–
412Z–
413Y+
413Z–
414Y–
414Z–
415Y+
415Z–
416Y–
416Z–
417Y+
417Z–
418Y–
418Z–
419Y+
419Z–
420Y–
420Z–
930229

Figure A-4.

REPORT DOCUMENTATION PAGE

Form Approved
OMB No. 0704-0188

1. AGENCY USE ONLY (Leave blank)	2. REPORT DATE	3. REPORT TYPE AND DATES COVERED
	June 1993	Technical Memorandum

4. TITLE AND SUBTITLE

Ground Vibration and Flight Flutter Tests of the Single-Seat F-16XL Aircraft With a Modified Wing

5. FUNDING NUMBERS

WU 533-02-35

6. AUTHOR(S)

David F. Voracek

7. PERFORMING ORGANIZATION NAME(S) AND ADDRESS(ES)

NASA Dryden Flight Research Facility
P.O. Box 273
Edwards, California 93523-0273

8. PERFORMING ORGANIZATION REPORT NUMBER

H-1906

9. SPONSORING/MONOTORING AGENCY NAME(S) AND ADDRESS(ES)

National Aeronautics and Space Administration
Washington, DC 20546-0001

10. SPONSORING/MONITORING AGENCY REPORT NUMBER

NASA TM- 104264

11. SUPPLEMENTARY NOTES

12a. DISTRIBUTION/AVAILABILITY STATEMENT

Unclassified—Unlimited
Subject Category 05

12b. DISTRIBUTION CODE

13. ABSTRACT (Maximum 200 words)

The NASA single-seat F-16XL aircraft was modified by the addition of a glove to the left wing. Vibration tests were conducted on the ground to assess the changes to the aircraft caused by the glove. Flight flutter testing was conducted on the aircraft with the glove installed to ensure that the flight envelope was free of aeroelastic or aeroservoelastic instabilities. The ground vibration tests showed that above 20 Hz, several modes that involved the control surfaces were significantly changed. Flight test data showed that modal damping levels and trends were satisfactory where obtainable. The data presented in this report include estimated modal parameters from the ground vibration and flight flutter test.

14. SUBJECT TERMS

Aeroelasticity, Flight flutter testing, Ground vibration testing

15. NUMBER OF PAGES

61

16. PRICE CODE

A04

17. SECURITY CLASSIFICATION OF REPORT	18. SECURITY CLASSIFICATION OF THIS PAGE	19. SECURITY CLASSIFICATION OF ABSTRACT	20. LIMITATION OF ABSTRACT
Unclassified	Unclassified	Unclassified	Unlimited

NSN 7540-01-280-5500 *For sale by the National Information Service, Springfield, Virginia 22161-2171*

Standard Form 298 (Rev. 2-89)
Prescribed by ANSI Std. Z39-18
298-102